

# High-resolution analysis of upper Miocene lake deposits: Evidence for the influence of Gleissberg-band solar forcing

Andrea K. Kern<sup>a,b,\*</sup>, Mathias Harzhauser<sup>a</sup>, Ali Soliman<sup>c,d</sup>, Werner E. Piller<sup>c</sup>, Oleg Mandic<sup>a</sup>

<sup>a</sup> Natural History Museum Vienna, Geological–Paleontological Department, Burgring 7, 1010 Vienna, Austria

<sup>b</sup> State Museum of Natural History Stuttgart, Paleontological Department, Rosenstein 1, 70191 Stuttgart, Germany

<sup>c</sup> University of Graz, Institute of Earth Sciences, Heinrichstrasse 26, 8010 Graz, Austria

<sup>d</sup> Tanta University, Faculty of Science, Geology Department, Tanta 31527, Egypt

## ARTICLE INFO

### Article history:

Received 19 June 2012

Received in revised form 5 December 2012

Accepted 8 December 2012

Available online 19 December 2012

### Keywords:

High-resolution analysis

Solar cycles

Palynomorphs

Lake Pannon

Miocene

## ABSTRACT

A high-resolution multi-proxy analysis was conducted on a 1.5-m-long core of Tortonian age (~10.5 Ma; Late Miocene) from Austria (Europe). The lake sediments were studied with a 1-cm resolution to detect all small-scale variations based on palynomorphs (pollen and dinoflagellate cysts), ostracod abundance, geochemistry (carbon and sulfur) and geophysics (magnetic susceptibility and natural gamma radiation). Based on an already established age model for a longer interval of the same core, this sequence can be limited to approx. two millennia of Late Miocene time with a resolution of ~13.7 years per sample. The previous study documented the presence of solar forcing, which was verified within various proxies on this 1.5-m core by a combination of REDFIT spectra and Gaussian filters. Significant repetitive signals ranged in two discrete intervals corresponding roughly to 55–82 and 110–123 years, fitting well within the lower and upper Gleissberg cycle ranges.

Based on these results, the environmental changes along the 2000-year Late Miocene sequence are discussed. No major ecological turnovers are expected in this very short interval. Nonetheless, even within this brief time span, dinoflagellates document rapid changes between oligotrophic and eutrophic conditions, which are frequently coupled with lake stratification and dysoxic bottom waters. These phases prevented ostracods and molluscs from settling and promoted the activity of sulfur bacteria. The pollen record indicates rather stable wetland vegetation with a forested hinterland. Shifts in the pollen spectra can be mainly attributed to variations in transport mechanisms. These are represented by a few phases of fluvial input but mainly by changes in wind intensity and probably also wind direction. Such influence is most likely caused by solar cycles, leading to a change in source area for the input into the lake.

Furthermore, these solar-induced variations seem to be modulated by longer solar cycles. The filtered data display comparable patterns and modulations, which seem to be forced by the 1000-year and 1500-year cycles. The 1000-year cycle modulated especially the lake surface proxies, whereas the 1500-year cycle is mainly reflected in hinterland proxies, indicating strong influence on transport mechanisms.

© 2012 Elsevier B.V. All rights reserved.

## 1. Introduction

Reliable documentations of high-frequency climate behavior, such as fluctuations in temperature or rainfall, reach back several hundred years only (Charvátová, 2000; Versteegh, 2005). This is clearly too short to allow convincing interpretations of the natural variations of climatic systems. Thus, high-resolution archives from the geological record may serve as additional sources of information. Especially in Holocene records, resolutions on decadal scales are abundant. Many of these suggest repetitive climate shifts strikingly similar to known variances of solar activity (e.g. Patterson et al., 2004; Solanki et al., 2004; Versteegh, 2005; Gray et al., 2010). Typically, the 11-year Schwabe-

cycle, the 22-year Hale-cycle, the 50–80-year lower Gleissberg cycle, the 90–120-year upper Gleissberg cycle, the ~210-year Suess/deVries cycle, and the 2200–2300-year Hallstatt cycle – along with the unnamed 500- and 1000-year cycles – are thought to have influenced the Holocene climate records (see Kern et al., 2012a for extensive discussion and references). Next to the famous radioactive isotope records of the Arctic and Antarctic ice cores (Stuiver and Braziunas, 1989, 1993; Beer et al., 1990, 2000; Damon and Sonett, 1991; Solanki et al., 2004), terrestrial and marine records document the presence of the influence of solar cycles around the globe. An early key discipline to discuss such external forcing was dendrochronology, where measurements of <sup>14</sup>C radioactive isotopes and the thickness of the tree rings mirror significant solar-related periodicities (Rigozo et al., 2002, 2008; Muscheler et al., 2004; Raspopov et al., 2004, 2008). Nevertheless, non-laminated lacustrine and marine sequences also revealed repetitive signals with comparable frequencies. This includes studies on isotopes (e.g. Cini Castagnoli et al., 2005;

\* Corresponding author at: State Museum of Natural History Stuttgart, Paleontological Department, Rosenstein 1, 70191 Stuttgart, Germany.

E-mail addresses: [andrea.kern@nhm-wien.ac.at](mailto:andrea.kern@nhm-wien.ac.at), [andrea.kern@smns-bw.de](mailto:andrea.kern@smns-bw.de) (A.K. Kern).

Taricco et al., 2009), pollen (Di Rita, 2011), nanoplankton (Incarbona et al., 2010) and multi-proxy data sets (Garcin et al., 2006). Still, aside from the better understood 11-year sunspot-cycle and the 22-year Hale-cycle, the origin of other cyclic variations in the sun's emitted energy remains unsolved (Versteegh, 2005). The sun's spin rate and rotation as well as the strength of solar winds are being discussed as explanations for longer-term variations, but the studies are inconclusive (Tsiropoulou, 2003). Nevertheless, all of the proposed longer solar cycles have been documented globally from various geochemical and sedimentological archives (Sonett and Suess, 1984; Raspopov et al., 2004). The expression and modulation of these cycles vary strongly in their local imprint (Hoyt and Schatten, 1997, 1998) and different responses on both hemispheres to the same cycle have also been noted (Li et al., 2001; Claud et al., 2008). This documents that the detection of the signals in the geochemical and sedimentological archives is comparatively easy while their explanation is not.

Comparable studies for the Miocene are scarce. Whereas the overall Neogene climatic history is well studied (e.g. Utescher et al., 2000, 2009; Zachos et al., 2001), small-scale shifts and short periods encompassing few thousands of years are usually unresolved. Recently, however, several high-resolution studies were conducted on Late Miocene sediments of Lake Pannon (Harzhauser et al., 2008; Gross et al., 2011; Paulissen and Luthi, 2011; Kern et al., 2012a,b). All detected high-frequency fluctuations of the paleo-environment of that lake

on a decadal scale. By using longer records, Gross et al. (2011) and Kern et al. (2012a) documented various repetitive patterns, which were linked to known periods of solar cycles. In addition, Kern et al. (2012a) showed how different proxies, such as magnetic susceptibility, natural gamma radiation and total abundance of ostracods, reflect the various cyclicities in individual intensities (Fig. 1). Periodicities of 50–80 (lower Gleissberg), 90–120 (upper Gleissberg), ~208 (deVries/Suess), 500, 1000, 1500 and 2300 years were described. All represent well-known solar cycles, except the 1500-year periodicity. Although the latter is well known from the Holocene, it seems to be de-coupled from solar forcing and is therefore labeled as an “Earth-system-immanent-cycle” (Bard and Frank, 2006; Debret et al., 2007, 2009). Importantly, the impact of this cycle on the sedimentation in the ancient Lake Pannon was one of the most prominent (Kern et al., 2012a, Fig. 1). No causal link between these observed changes in environmental conditions, as expressed by the proxy data and the suggested solar forcing, has been forwarded. To better elucidate the interaction between the environment, the climate and the presumed solar cycles, we conducted a further study based on the data presented in Kern et al. (2012a) and new data on pollen, dinoflagellates, molluscs, total carbon (TC), total organic carbon (TOC), and total sulfur (TS).

These proxy-data provide information on the vegetation surrounding the lake (pollen), climate (pollen), surface water productivity (dinoflagellates), lake bottom conditions and on the overall sediment input

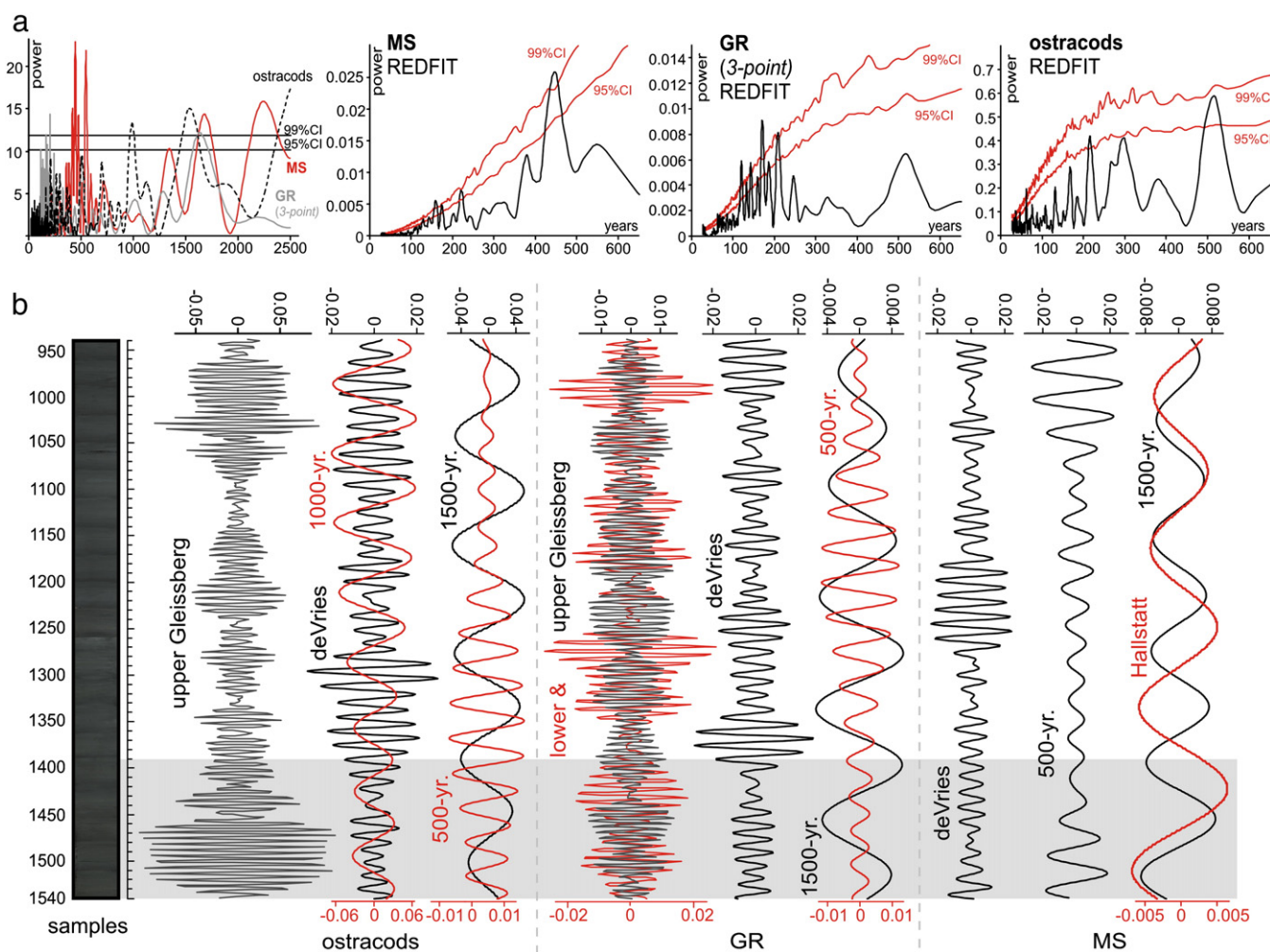


**Fig. 1.** A summary of the assumed solar cycles in the 6-m-long Hengersdorf core from Kern et al. (2012a). (a) Combined Lomb–Scargle periodograms of MS (magnetic susceptibility; red), GR (natural gamma radiation; gray) and the total abundance of ostracods (dashed) and REDFIT spectra. (b) Filtered records based on dominant frequencies as revealed by spectral analysis (modified from Kern et al., 2012a). Each filtered curve is labeled with the corresponding solar cycle (lower Gleissberg, upper Gleissberg, deVries, 500-year, 1000-year, Hallstatt cycle as well as the 1500-year cycle of unknown origin). The shaded area indicates the herein analyzed interval.

(ostracods, molluscs, magnetic susceptibility, natural gamma radiation, TC, TOC, TS).

## 2. Geological setting

The Late Miocene to Pliocene Lake Pannon covered the Pannonian Basin complex in central and south-eastern Europe (Fig. 2). It formed at c. 11.6 Ma when the marine Paratethys Sea retreated to the east. The remaining lake was a brackish and slightly alkaline lacustrine system (Magyar et al., 1999; Harzhauser et al., 2004; Piller et al., 2007; Harzhauser and Mandic, 2008). During the herein discussed phase at c. 10.5–10.4 Ma, Lake Pannon experienced its maximum extension (Fig. 2d) and deep basins with dysoxic conditions were established. At that time, pelitic sediments of the Bzenec Formation were deposited in the entire Vienna Basin (Harzhauser et al., 2004).

The studied core was taken at the clay pit Hennesdorf (Fig. 2c) app. 10 km south of the center of Vienna in the Vienna Basin (N48°05'52.6", E016°21'15.8", 186 masl). There, more than 20 m of dark-gray to greenish clay and silt of the Bzenec Formation crop out. Its mollusc fauna indicates the regional middle Pannonian stage, corresponding to the middle Tortonian (Magyar et al., 1999), a dating further supported by magnetostratigraphy (chron C5n, Magyar et al., 1999). The succession can be correlated with astronomically tuned well-logs in the Vienna Basin, suggesting an absolute age of c. 10.5–10.4 Ma (Harzhauser et al., 2004; Lirer et al., 2009). A first

study by Kern et al. (2012a) was conducted on a continuous 6-m-long core with homogeneous sediment. Occasionally, scattered plant debris and autochthonous mollusc coquinas were present, whereas bioturbation was exceptionally rare. Kern et al. (2012a) documented a rather constant sedimentation rate ranging around 0.73 mm/year for this part of the drilling. This corresponds to a hypothetical time resolution of 13.7 years/cm, which represents the applied sample density. More detailed information on the lithology, paleontology and biostratigraphy of the Hennesdorf section has been published by Harzhauser and Mandic (2004), Harzhauser et al. (2008) and Kern et al. (2012a).

## 3. Methods

In November 2009, several consecutive cores with a diameter of 15 cm were drilled, reaching a depth of 15.4 m. The lowermost part was taken without core-break and is the most uniform part with respect to lithology. Therefore, further analyses concentrated on this deepest segment (see Kern et al., 2012a for details and sampling protocol). After cutting the core into identical two halves, geophysical measurements were conducted in a strict 1-cm-sample-interval including natural gamma radiation (GR) with a hand-held Scintillation Gamma Radiometer and magnetic susceptibility (MS) with a "SM-20" magnetic susceptibility meter with a sensitivity of  $10^{-6}$  SI units (GF Instruments, Brno, Czech Republic). Afterwards, the core was cut into slices, following

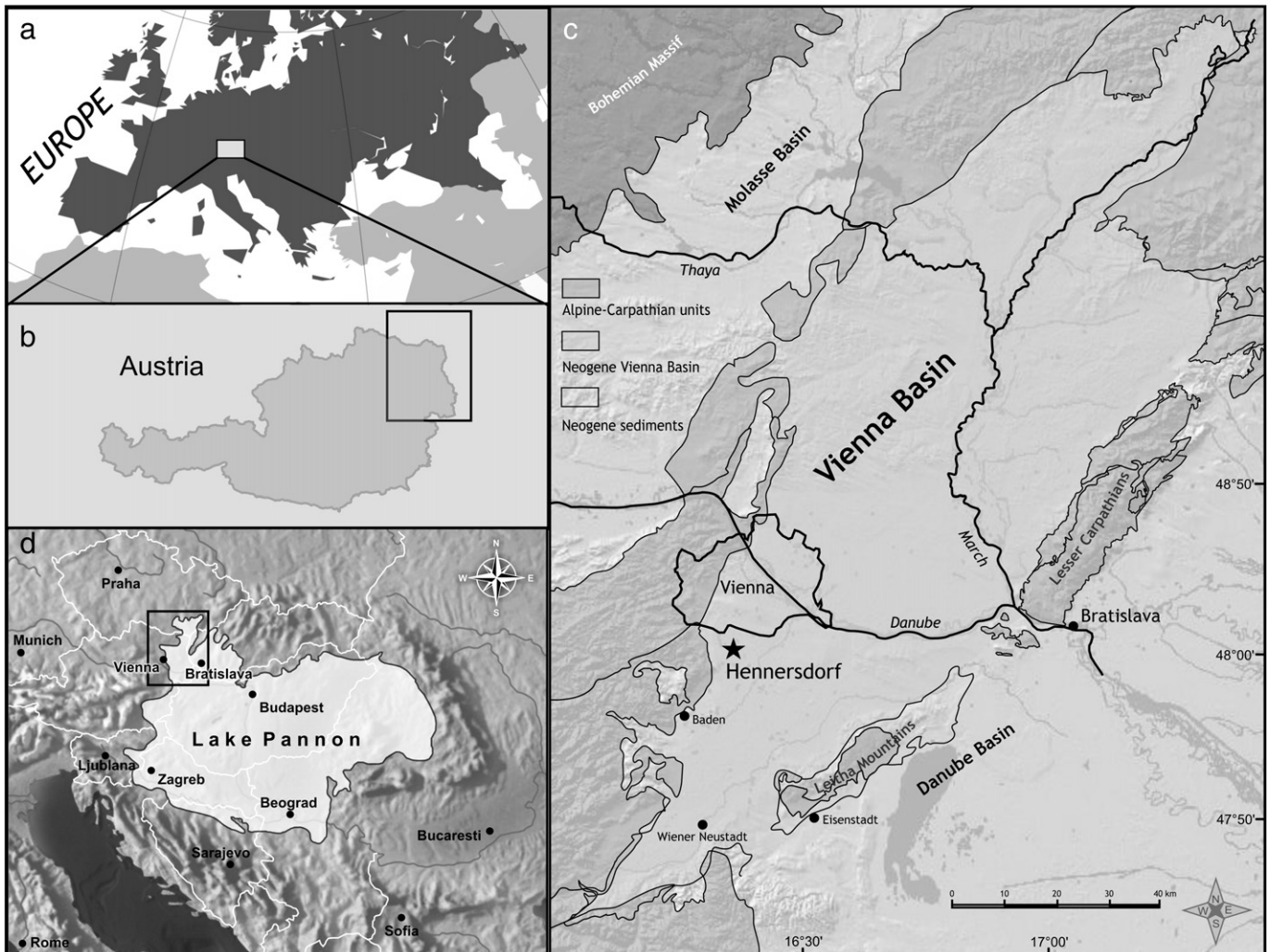


Fig. 2. Map showing the study area in central Europe (a) and Austria (b). The outline of the Vienna Basin is presented in inset c and the drilling site is marked by an asterisk. Inset d shows the position of inset c based on a paleogeographic map of Lake Pannon at ~10.5 Ma (modified from Magyar et al., 1999; Harzhauser and Mandic, 2008).

the same 1-cm-sampling protocol, and immediately separated for the different analyses (palynology, ostracods, molluscs and geochemistry). Ostracod samples were dried, weighed and treated with H<sub>2</sub>O<sub>2</sub> before sieving with 125, 250 and 500 µm mesh-size sieves. The total number of ostracod valves was evaluated first, before data were standardized for a sample weight of 100 g (Supplementary Table 1). For statistical analyses, these data were log-transformed. Molluscs were picked from the identical samples as well. As the shells were fragmented during washing, no individual numbers were counted. Therefore, the abundance of molluscs was evaluated by using semi-quantitative categories: 0 = no fragments at all, 1 = rare fragments, 2 = frequent shell fragments, and 3 = coquina layers with numerous fragments.

The geochemistry was measured using a Leco CS-300 elemental analyzer at the University of Graz, detecting total sulfur (TS), total carbon (TC) and total organic carbon (TOC, after acidification of samples to remove carbonate). The difference between TC and TOC is the total inorganic carbon content (TIC), which was used to calculate calcium carbonate equivalent percentages ( $c\text{-equi} = 8.34 \cdot \text{TIC}$ ).

Preparation of the palynological samples (pollen, spores and dinoflagellate cysts) followed the steps of Wood et al. (1996) and Green (2001). Each sample was dried, weighed and one *Lycopodium clavatum* tablet was added to calculate the absolute number of pollen and dinoflagellate cysts. Then it was treated with cold HCl (34%) to remove all carbonate. After washing with distilled water, each sample was treated with HF (48%) and cold HCl to fully remove all silicates and colloids. The residue was ultrasonicated (c. 15–30 s) and colored with Safranin O, before it was sieved at 15 µm with a nylon sieve. In each sample, at least c. 250 dinoflagellate cysts and 200 pollen grains (excluding *Pinus*) were identified. Palynological counting was first transferred to percentages before an arcsin-root transformation was applied for further statistics (Linder and Berchtold, 1976; Zúschin and Hohenegger, 1998). For the pollen, a standard Tilia diagram was created (Grimm, 2004). To generate a paleoclimate estimate, the Coexistence Approach was used (Mosbrugger and Utescher, 1997). The method applies the natural distribution of the nearest living relative of each taxon occurring in the fossil assemblage, and transfers this to a possible climatic interval in which all of these Miocene plants could survive today. This climatic range is called the Coexistence Interval and resembles the most likely prevailing climatic conditions. Far-transported pollen grains as well as pollen grains of species with a recent distribution strongly influenced by human activity may not characterize the natural distribution or the paleo-situation. To not avoid a mix of climate of different altitudes, such taxa were therefore excluded from the list before the method was applied (e.g. *Pinus*, *Abies*, *Picea*, *Cathaya*). All details referring to Coexistence Approach are summarized in Supplementary Table 2.

To detect and describe cyclicities, a combination of the software PAST (Hammer et al., 2001) for REDFIT analysis (Schulz and Mudelsee, 2002) and the software AnalySeries (Paillard et al., 1996) for filtering was used. REDFIT overcomes the common problem in paleontology of unevenly spaced time series by fitting a first-order autoregressive process. It also helps reduce red noise by using segmentations and oversamples to fit each curve to a noise model. The Monte-Carlo method was applied to test a bias-corrected spectrum. Only peaks above the 95% confidence interval in the REDFIT spectrum were considered. The age model and the sample numbering follow Kern et al. (2012a), with a sedimentation rate of 13.7 years/cm, thus representing 13.7 years in between each sample.

## 4. Results

### 4.1. Pollen

A pollen diagram was generated showing the most common plant taxa, and a pollen zonation is proposed based on cluster analysis (Fig. 3a). The diversity of the pollen assemblage was rather low,

ranging from 13 to 34 taxa (Fig. 3b; Supplementary Table 1). Moreover, the diversity decreased from the bottom of the core (1540) to the top, but the gradient became less steep above sample 1490. The pollen number per gram sediment, based on the *Lycopodium clavatum* counts, was basically high with one exceptional peak of 97,880 in sample 1500; values never fell below 12,300. The values increase moderately from the bottom to a peak at sample 1521, followed by a break-down phase to values between 30,000 and 20,000. Afterwards, a quick increase causes the highest peaks at sample 1500, which passes into a strongly fluctuating interval up to sample 1476. This interval shows no trend and has a mean of c. 40,700 pollen/g. Subsequently, values drop distinctly starting from sample 1476 and display an overall decreasing trend with very low values of 14,000–16,000 pollen/g up to about sample 1420. Afterwards the number increases slowly again. The pollen/gram record (Fig. 3b) was not correlated with the pollen diversity curve. Both lack a significant correlation with the dinoflagellates/gram record. This suggests that most of the data are not taphonomically biased, which would affect all palynomorphs.

As *Pinus* accounts for up to 50% of the whole pollen spectra (Fig. 3b), it was excluded from further analysis. The decrease in diversity coincides with an increase in the abundance of gymnosperm pollen (excluding *Pinus*). Starting from 60%, the values reach c. 90% in samples 1491 and 1405 (Fig. 3b). Among the remaining bisaccate gymnosperms, *Cathaya* is most abundant with values of almost 50% and a mean of 38.2% (Fig. 3a; Supplementary Table 1). *Picea* and *Abies* attain lower mean values of 14.4% and 14.6%, respectively. *Picea* displays three peaks with 25%, which slightly exceed the three *Abies* peaks. Despite the comparable values, all three Pinaceae records have different patterns (Fig. 3a). *Cathaya* strongly increases from sample 1540 up to sample 1494 (50.6%), before it slightly drops to 31% up to sample 1472. Afterwards, the *Cathaya* record varies strongly with positive and negative peaks between 50 and 30%. *Abies* and *Picea*, in contrast, start with rather stable values and peak later at samples 1480 (21%) and 1473 (26%). *Picea* values briefly drop down to less than 10%, before they increase slowly up to sample 1430 (24.4%), followed by an interval without a significant trend. *Abies* also decreases to values around 7.6%, followed by a slight increase to between 10 and 15%, with a negative peak at sample 1432 (5.6%). A strong rise up to 18% afterwards is followed again by a short decrease down to 10%. In the top of the sequence, the abundance of *Abies* increases, similarly to *Picea*, but displays a decreasing trend after sample 1403 (23.7%).

The rather rare angiosperms were grouped according to their ecology into hinterland forest and grasses/herbs (comparable to Jiménez-Moreno, 2006; Kovar-Eder et al., 2006; Jiménez-Moreno and Suc, 2007; Fig. 3b; for the complete taxa list, see Supplementary Table 1).

The hinterland forest plants are more abundant, ranging from 5.9% to 19.3%, with their highest values in the lower part (1540 to 1525) and in the middle (1469 to 1460), opposed by one negative peak at sample 1405 (5.9%). They start with a negative trend up to sample 1525; the interval up to sample 1432 is characterized by high values, with two phases exhibiting several positive peaks (1503–1516, 1477–1455) and a decline afterwards up to sample 1432; this marks the turning point to overall increasing values (Fig. 3b). Grasses/herbs start with values of almost 19% and sharply decrease to 3.9% at sample 1531. This is followed by a slight recovery up to sample 1528 (8.7%) and a second but less steep negative trend up to sample 1500. Rather low values without marked trend follow upsection, interrupted only at sample 1468, when grasses and herbs attain 10.8% of the spectrum (Fig. 3b).

### 4.2. Dinoflagellate cysts

The diversity of dinoflagellate cysts is low in all samples; a total of 17 taxa were identified (Fig. 4; Supplementary Table 1). The most abundant is *Spiniferites* with values up to 60%. Five different species

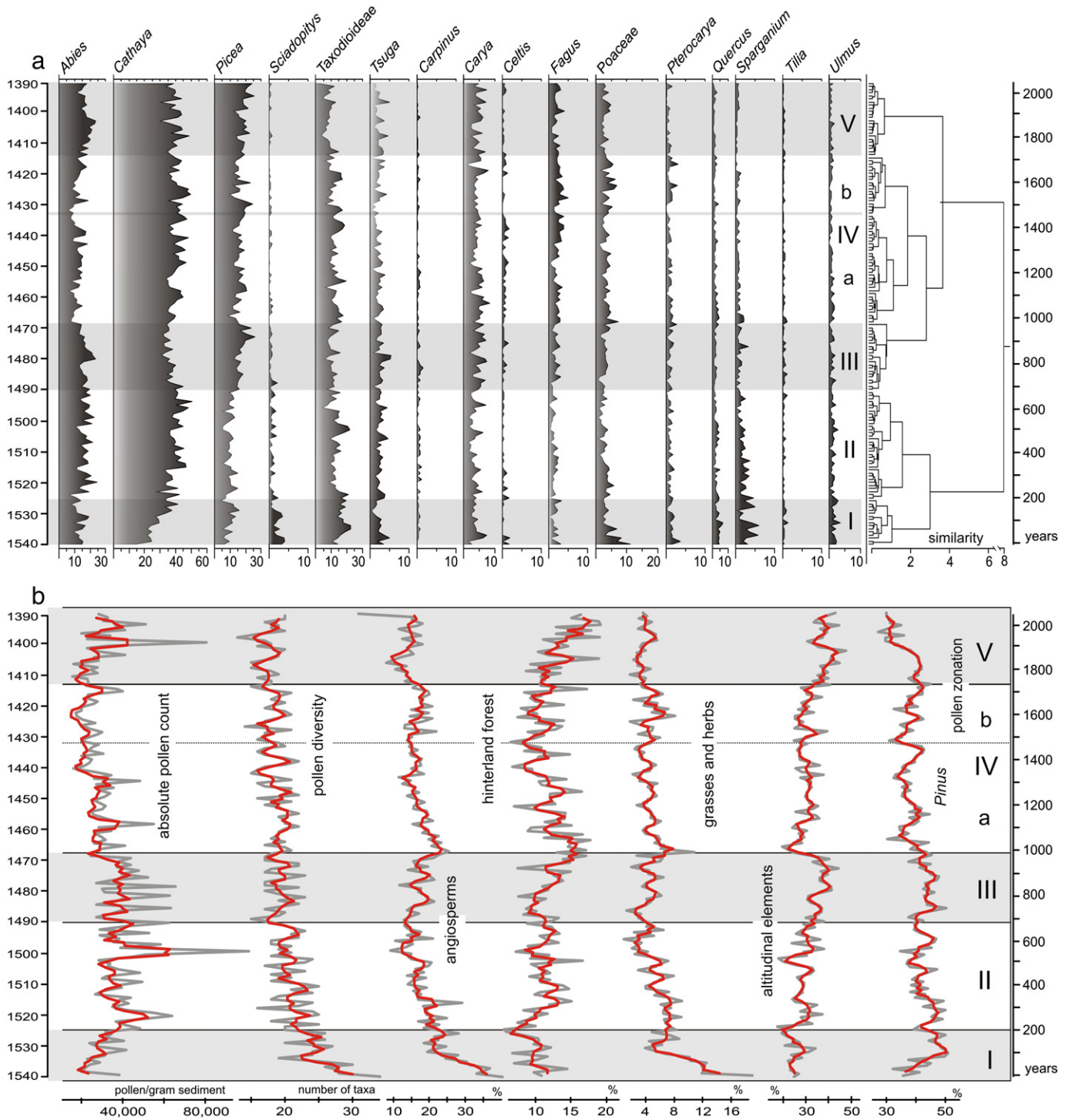


**Fig. 3.** Panel (a) represents a classic pollen-diagram generated with the Tilia program (Grimm, 2004) showing the most common taxa and a pollen zonation based on CONISS (this zonation is also used in b – 8). All remaining taxa are less abundant and are excluded from the graph (see Supplementary Table 1 for a total abundance list). Diagrams in b show the amount of pollen per gram sediment (absolute pollen counts), pollen diversity (number of taxa identified), angiosperms (%), forest elements (%; *Acer*, *Alnus*, *Betula*, *Carpinus*, *Carya*, *Castanea*, *Celtis*, *Engelhardia*, *Fagus*, *Ilex*, *Juglans*, *Liquidambar*, *Platycarya*, *Pterocarya*, *Quercus*, *Tilia*, *Ulmus*, *Zelkova*), grasses and herbs (%; *Amaranthaceae*, *Artemisia*, *Asteraceae*, *Caryophyllaceae*, *Chenopodiaceae*, *Cyperaceae*, *Ephedra*, *Poaceae*, *Sparganium*, *Typha*), altitudinal elements (%; *Abies*, *Picea*, *Tsuga*) and *Pinus* (%) in relation to the pollen zonation (a). Gray lines represent raw data, red lines show the 3-point mean. *Pinus* was not considered for any pollen calculation except to generate the *Pinus* curve itself.

are identified within this genus: *Spiniferites delicatus* is the most common, frequently accounting for more than 10% of the assemblages and with a single peak topping 32% in sample 1479. All other *Spiniferites* species range below 5% with mean-values of less than 1.5% (Supplementary Table 1). The second most frequent element is *Impagidinium* spp. with maxima of 36.7% and a mean of 20.7%.

*Impagidinium sphaericum* ranges from 2 to 18.3% (mean 7.8%). Among the remaining taxa, especially the Protoperidinioid cysts A and Round Brown Cysts (RBC) are most common with a mean of 33.7% and maxima of 18.0%, respectively. *Pyxidinospis psilata* and *Selenopemphix* sp. are also constantly present with means of 2.8% and 2.2%, respectively.

*Spiniferites* values show a decreasing trend up to sample 1515. This is followed by a strongly fluctuating overall increase up to sample 1470, attaining a peak value of 55.7%. During the following six samples, a strong drop to 29.3% occurs. Upsection, a constant increasing trend follows, peaking at sample 1443 (55.5%), followed by overall constant values around 45% until sample 1433. A short phase of low values around 35% up to sample 1428 is opposed by the highest peak at sample 1426 (60.6%). Another phase of low values up to sample 1412 is finally topped by a slight increase to values around 40% (Fig. 4). *Impagidinium* spp. starts with slightly increasing values, peaking at sample 1508 with 48%. At sample 1504, values drop to 18% and further to 15.4% in sample 1492 after a short recovery phase. Afterwards it is consistently represented in samples, varying between 20% and almost 40%. At sample 1462, values increase again to a peak at sample 1446 (43.3%). Upsection, another phase of strongly fluctuating values follows, indicating a slight decreasing trend up to sample 1426 and an increase in abundance thereafter. A clearer trend is expressed by the *Protoperidinioid* cyst A (Fig. 4). Its values increase constantly from samples 1540 to 1517, peaking at 26.7%. This trend is interrupted by a short break-down phase to 11.6% at sample 1506, before the increasing trend is re-established, peaking at sample 1491 with 33.4%. Values decrease irregularly into a low phase of c. 12% from samples 1473 to 1470. This is followed by peak values of more than 30% around samples 1467 to 1465. Afterwards, the *Protoperidinioid* cyst A assemblage decreases considerably down to 3.4% (samples 1453–1535) and terminates with strongly fluctuating values. RBC start with an increase from about 2% towards a phase of high peaks of 8–10% between samples 1515–1505. Afterwards, the abundance drops again below 5% up to sample 1468, where a strong rise takes place up to a last drop at sample 1401. Nevertheless, values fluctuate considerably in between, including shifts from 0% to more than 15% within several samples. *Selenopemphix* shows a rather characteristic behavior along the sequence. From sample 1540 until 1525, it is more abundant (peaks >6%), before it breaks down to values <3%. Although small shifts are still evident, the occurrence remains low until sample 1400, where values exceed 12%. *Pyxidiniopsis* shows a more variable trend, beginning with an almost stable presence around 2% up to sample 1401, where the values rise to 4.5%. After a short drop, the values slowly increase towards the highest

abundance at sample 1442 (8.3%), before they fall constantly towards a low at sample 1433 (1.5%). The signal towards the top of the sequence remains highly fluctuating, but with an increasing trend including one more peak of 8.5% (1396).

#### 4.3. Ostracod and mollusc abundance

We use the total amount of ostracods and the presence of autochthonous mollusc populations as rough estimates for bottom water conditions; for a discussion on the species and genera constituting the assemblage see Harzhauser and Mandic (2004) and Harzhauser et al. (2008). Within the studied core interval, the maximum abundance of ostracods/100 g sediment is observed from samples 1540 to 1525 (Supplementary Table 1; Fig. 5). Afterwards the assemblages break down nearly completely up to sample 1513, followed by a phase of strongly fluctuating values ranging from 10 to almost 300 individuals, with a low phase of <60 ostracods between samples 1414 and 1400.

#### 4.4. Geochemistry

The total sulfur record (TS) displays an overall two-parted trend with higher values up to sample 1475 and depleted values thereafter (Supplementary Table 1; Fig. 5). The lower part of the core up to sample 1475 has strongly fluctuating values around a mean of 0.47%, with several prominent peaks of >0.8%. Above follows a phase with low fluctuations and a constant decline to low values around 0.2% up to sample 1443. These depleted values continue up to the top of the core, interrupted only by a short interval of slightly higher values from samples 1443 to 1430.

Total carbon values (TC) range between 1.75 and 2.6% (Supplementary Table 1; Fig. 5). The lower part of the core up to sample 1530 is characterized by high values with peaks of 2.5 and 2.6% in samples 1539 and 1534. This is followed by an interval up to sample 1457 with moderate values fluctuating around 2%, with a phase of very low values around 1.7% around sample 1500 and a slight increasing trend afterwards. Elevated values occur in an interval from samples 1455 to 1438, followed again by phase of moderately fluctuating values ranging around 2%.

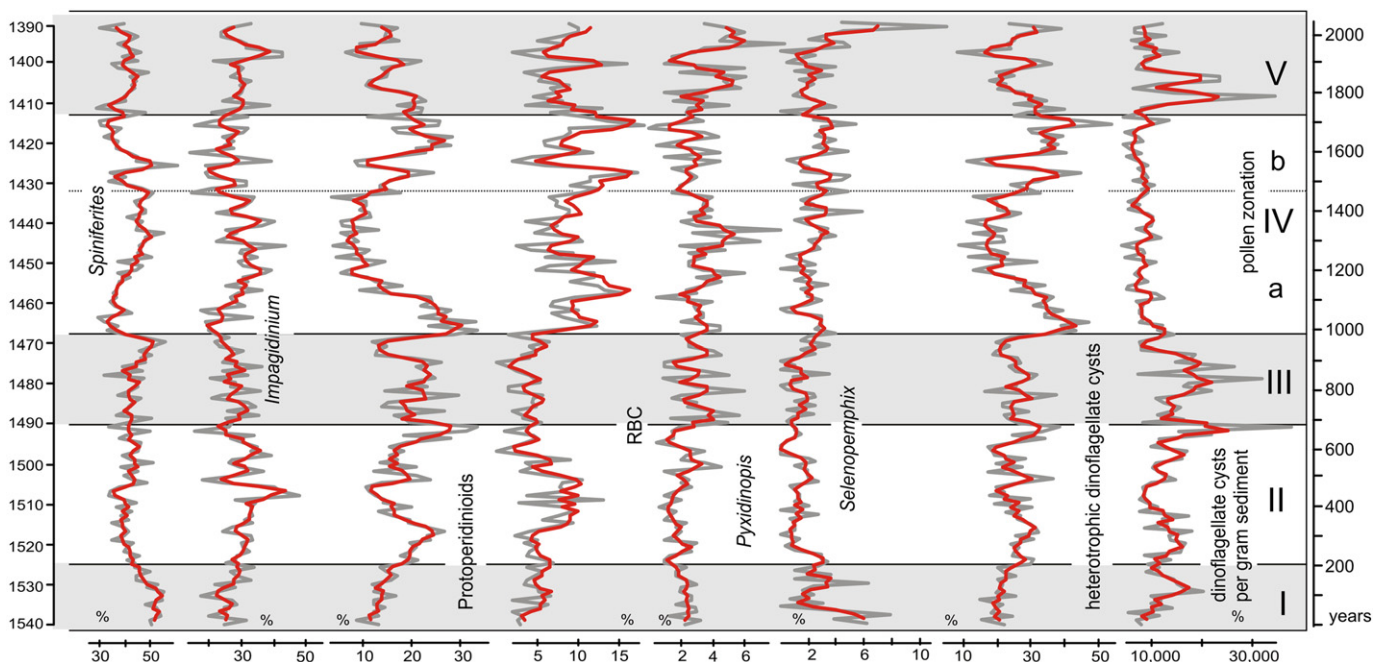


Fig. 4. The six most important dinoflagellate cyst taxa (RBC = Round Brown Cysts), the total heterotrophic dinoflagellates and the number of cysts per gram sediment in relation to the pollen zonation (Fig. 3a). Gray lines represent raw data, red lines show the 3-point mean.

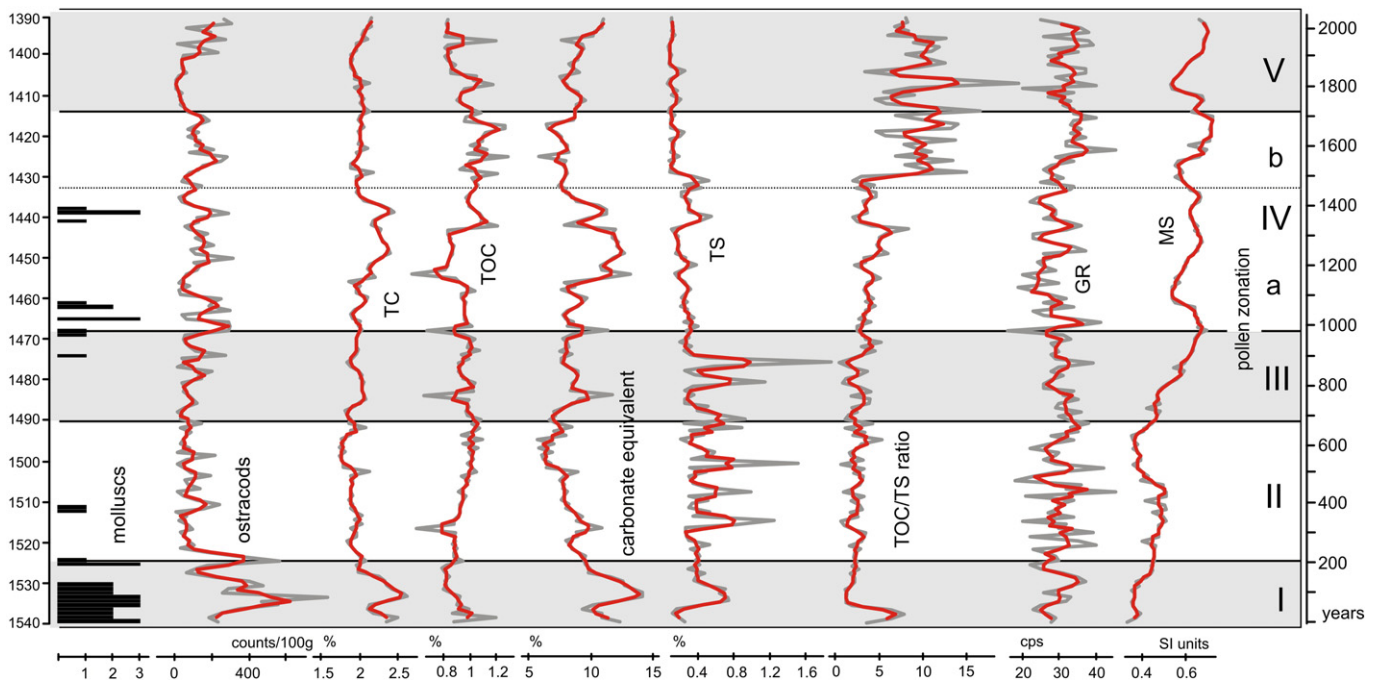


Fig. 5. Paleozoological (molluscs, ostracods), geophysical (MS = magnetic susceptibility, GR = natural gamma radiation) and geochemical proxies (TC = total carbon, TOC = total organic carbon, TS = total sulfur) in relation to the pollen zonation (Fig. 3a). Gray lines represent raw data, red lines show the 3-point mean.

The total organic carbon record (TOC) is also two-fold: the lower part reaches from the bottom up to sample 1444 (Supplementary Table 1; Fig. 5). This part is characterized by an overall mean of 0.92%, separated by moderately increasing values up to sample 1490 and a slight decrease afterwards. Four prominent negative peaks interrupt this record at samples 1517 (0.6%), 1484 (0.64%), 1468 (0.68%) and 1454 (0.56%). The upper part of the TOC record has comparatively higher values, with a mean of 1.0%, starting with a strong increase at sample 1442.

The trend of the calcium carbonate equivalent is roughly similar to the TC record because its calculation is based on TC and TOC values (Supplementary Table 1; Fig. 5). Comparable to the TC record, an initial phase with high values up to sample 1530 is followed by a constant decrease, which culminates in low values around sample 1500. Afterwards a slow but constant increasing trend with positive peaks at samples 1484 (11.7%) and 1468 (11.3%) sets in. An interval with very high values around 1% occurs up to sample 1435. This interval ends with an abrupt decrease, followed by a constant rise up to the top afterwards.

The TOC/TS ratio starts with its first peak of 7.8% within the first 5 samples and then remains at low levels of app. 3% up to sample 1495, when the values display a moderate increase with several peaks up to almost 5%. Around sample 1473 the values increase further, interrupted by a short phase of low values from samples 1440–1431. Afterwards, the ratio displays an overall shift towards higher values, with maxima of 20% and an average of 10%.

#### 4.5. Geophysics

The natural gamma radiation (GR) of the 6-m-long Hennersdorf core was already discussed by Kern et al. (2012a). The shorter herein-studied part is characterized by a strongly fluctuating record (Supplementary Table 1; Fig. 5) with increasing amplitudes up the interval between samples 1520 and 1500. An interval with low-amplitude variations reaches up to the interval around sample 1470, where strong positive and negative peaks occur. A phase of moderate fluctuations follows and extends up to sample 1425, then passing quickly into a last interval with elevated and strongly fluctuating values.

As shown by Kern et al. (2012a) the magnetic susceptibility record (MS) lacks the high-frequency oscillations of the GR record. The magnetic susceptibility shows a trend of increasing values towards the top of the section from  $0.3$  to  $0.6\text{--}0.7 \times 10^{-6}$  SI units, with a low-frequency fluctuation. The strongest increase occurs between samples 1495 and 1470. Other fluctuations are minor (Supplementary Table 1; Fig. 5).

#### 4.6. Statistics

The longer sequence of 6 m studied in Kern et al. (2012a) already exhibited periodicities in the magnetic susceptibility (MS), natural gamma radiation (GR) and ostracod records (Fig. 1) that fit to those of the lower and upper Gleissberg cycles (50–80 and 90–120 years), the deVries/Suess cycle (200–210 years), the 500- and 1000-year cycles and the Hallstatt cycle (~2300 years). Additionally, a strong influence of the 1500-year cycle could be detected for these 3 proxies. The same techniques were applied for each proxy herein, but due to the shorter time interval of c. 2055 years, only the lower and upper Gleissberg and the deVries/Suess cycles are expected to be present. Shorter cyclicalities, such as the 11-year-Schwabe-sunspot cycle or the 22-year-Hale cycle, approximate the time resolution between each sample and thus cannot be detected (Hoyt and Schatten, 1998; Versteegh, 2005; Gray et al., 2010). Accordingly, with respect to the time model of 13.7 years/cm, only a part of the frequency spectrum can be considered. Very low frequencies ( $\leq 0.05$ ) may not show enough repetitions within the investigated sequence, and high frequencies  $\geq 0.3$  are too close to the time resolution.

In the following we give a short overview of significant periodicities as revealed by REDFIT spectral analysis (Schulz and Mudelsee, 2002). Eleven proxies revealed signals above the 95% confidence interval: GR, carbonate, TS, Protoperidinoid cyst A, *Impagidinium*, Round Brown Cysts, *Picea*, *Cathaya*, Poaceae, *Fagus* and ostracods (Fig. 6a–k). Several others indicate peaks at comparable frequencies, but did not reach the 95% CI and are not discussed herein.

GR (Fig. 6a): three peaks between the frequencies of 0.167–0.173, 0.213–0.22 are detected next to one peak at 0.273, which appears to be a split signal with respect to the many following peaks passing the

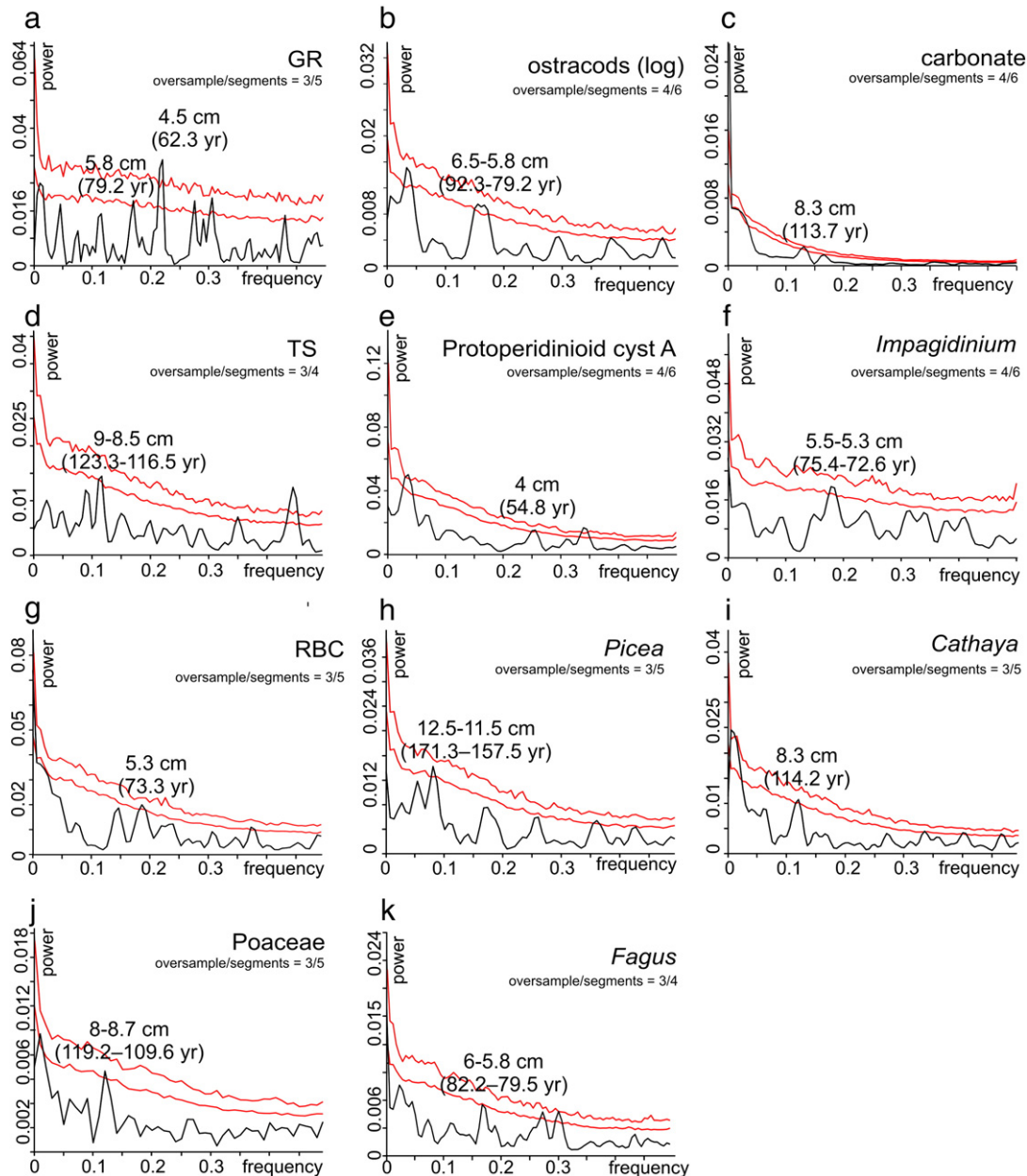


**Fig. 6.** REDFIT periodograms of 11 proxies with significant peaks passing the 95% confidence interval (lower red line; upper line represents 99% CI), including the oversample/segment numbers used to reduce red noise (Schulz and Mudelsee, 2002). Abbreviations used: GR=natural gamma radiation, TS=total sulfur, RBC=Round Brown Cysts. Frequencies are converted to cm for easier comparison.

frequency limit of 0.3. Therefore, the value of the highest peak is uncertain. The two remaining peaks correspond to a repetitive signal of 6.0–5.8 and 4.7–4.5 cm and 82.0–79.2 and 64.3–62.3 years in time.

Ostracods (Fig. 6b): one prominent peak above the 95% CI occurs at a frequency between 0.148 and 0.173, which can be expressed as a repetitive signal with a periodicity of 6.8–5.8 cm and 92.3–79.2 years.

Carbonate (Fig. 6c): one peak at the frequency 0.12 almost passes the 99% CI, while a second one at 0.18 frequency reaches the 95% CI. These represent 8.3 cm (113.7 years) and 5.6 cm (76.7 years), respectively.

TS (Fig. 6d): one peak at frequencies between 0.111 and 0.117 exceeds the 95% CI; this corresponds to 9.0–8.5 cm or 123.3–116.5 years. A second peak at 0.089 does not reach the 95% CI but might represent a split peak of the same signal.

Protoperidinioid cyst A (Fig. 6e): only one wide peak reaches above the 95% CI at the frequency between 0.247 and 0.25, corresponding to a cyclicity of 4.0 cm or 54.8 years.

*Impagidinium* (Fig. 6f): several peaks are visible, but only one at the frequency 0.183–0.189 is strong enough to pass into the 95% CI; it corresponds to a frequency of 5.5–5.3 cm or 75.4–72.6 years.

Round Brown Cysts (Fig. 6g): several peaks are visible but only at a frequency of 0.187 is the 95% CI passed. This means a cycle of 5.3 cm or 73.3 years.

*Picea* (Fig. 6h): this pollen shows a rather weak peak at a frequency of 0.08–0.087, corresponding to 12.5–11.5 cm or 171.3–157.5 years. All higher frequency signals fail to reach the 95% CI.

*Cathaya* (Fig. 6i): within this spectrum, many high frequency signals occur, but only one the one at 0.12 passes the 95% CI value, corresponding to 8.3 cm or 114.2 years.

Poaceae (Fig. 6j): a clear frequency peak at 0.12–0.125 is present, which corresponds to 8.7–8.0 cm or 119.2–109.6 years.

*Fagus* (Fig. 6k): REDFIT detects several peaks within this data set; first at 0.167–0.172 and two identical neighboring peaks at 0.267–0.27

and 0.29–0.3. Since these two peaks are equally strong, they are presumably the result of a split signal. As the tops of these frequency peaks pass the significance limit of 0.3, they are excluded from further analysis. The remaining peak at 0.167–0.172 corresponds to 6.0–5.8 cm or to 82.2–79.5 years. With respect to the whole number of proxies counted and measured for this 1.5 m sequence, the number of statistically significant ones is low. This mainly reflects the small sample size of 150 data points per proxy and the quasi-periodic nature of solar cycles. In comparison, the GR, MS and ostracod records show a clearer signal in the studies of Kern et al. (2012a) by applying the same technique on a larger data set. Therefore, the irregularity in the exact duration of each solar cycle marks the biggest obstacle for studying these based solely on a short sequence. Furthermore, several other pollen taxa also reflect repetitive abundance patterns, but these were excluded because they all represent very rare elements (e.g. *Tilia*, *Arecaceae*, *Ericaceae*, and *Rosaceae*). The signal in the statistics may reflect presence/absence only: this might indicate a taphonomic signal, but could also be caused by the offshore position of the studied core.

Summarizing the detected frequencies, the significant peaks cluster in two discrete intervals of 4–6 and 8–9 cm, representing 54.8–82.2 and 109.6–123.3 years. These values range well within the expected ranges of the lower Gleissberg cycle (50–80-year period; Ogurtsov et al., 2002; de Jager et al., 2010) and the upper Gleissberg-cycle (90–120-year period; Wolf, 1862; Gleissberg, 1939; Ogurtsov et al., 2002). These results are apparently robust because Harzhauser et al. (2008) and Kern et al. (2012a) detected comparable peaks within the lower and upper Gleissberg frequency bands in core intervals below and above the herein-studied interval.

Only the single *Picea* peak of roughly 170–160 years does not fit to any known cycles. It could possibly be a heterodyne of the Gleissberg cycle with the ~200 year deVries solar cycle. Since its expression is rather weak and its presence cannot statistically be substantiated by any other proxy, it will not be considered for further discussion.

## 5. Discussion

### 5.1. General paleoclimate

The general paleoclimate for the Hennersdorf locality was estimated based on 32 taxa by applying the Coexistence Analysis (Supplementary Table 2). The results suggest a mean annual temperature (MAT) between 15.6 and 20.8 °C, with a cold season clearly above the freezing level (5–13.3 °C) and a warm season range from 24.7 °C to 27.9 °C. The mean annual precipitation (MAP) was high, varying from a low of 823 up to 1529 mm, displaying clear seasonality with a wet phase of 204–236 mm and a dry phase of 9–24 mm. As the warmest month, rainfall ranged from 79 to 172 mm, the warmer season may have coincided with the wettest one (Supplementary Table 2). Thus, a clear seasonality was already established at this time, with a cold and a warm and presumably wetter season. Rainfall and temperature suggest a subtropical or at least warm-temperate situation compared to today (e.g. Vienna — MAT 9.8 °C and MAP 660 mm; Müller, 1996). The warm temperature and especially the winter temperature above 0 °C is responsible for the presence of plants that today are typical for tropical and subtropical areas, such as *Arecaceae*, *Sapotaceae*, *Engelhardia* or *Taxodiaceae* (Denk et al., 2001; Kvaček, 2007; Kunzmann et al., 2009). These data fully correspond to previous studies from other nearby localities (Bruch et al., 2004, 2006; Harzhauser et al., 2008; Jiménez-Moreno et al., 2008).

### 5.2. Vegetation reconstruction

Due to the low diversity within the pollen assemblages, only a rough picture of the Late Miocene vegetation surrounding Lake Pannon can be reconstructed. The lakeshore was probably fringed by a mixture of

forested and non-forested wetland vegetation. There, different *Poaceae* and *Cyperaceae* species occurred, partly associated with *Sparganium* and *Typha*. Typical trees of this zone were *Taxodiaceae*, such as *Taxodium* or *Glyptostrobus*, along with the less frequent *Nyssa* (e.g. Willard et al., 2001; Averyanov et al., 2009; Kunzmann et al., 2009; Lodge, 2010). Due to their high frequency in the spectra and the fact that their pollen grains are usually not transported over large distances (Smirnov et al., 1996), the presence of such lakeshore-associated wetlands is most likely, although some species of *Taxodiaceae* may grow in non-swamp vegetation as well (e.g. Thompson et al., 1999). In some distance from the lakeshore, forests dominated the landscape. This part of the vegetation comprised mainly deciduous, broad-leaved type taxa (Kovar-Eder et al., 2008). This included elements such as *Carya*, *Pterocarya*, *Quercus*, *Fagus*, *Carpinus* or *Ulmus*, together with some plants typical for warm-temperate climate such as *Arecaceae* and rare occurrences of *Symplocos* or *Sapotaceae* (e.g. Jarvis and Clay-Poole, 1992; Britton and Crivelli, 1993; Wilen and Tiner, 1993; Denk et al., 2001; Kováčová et al., 2011). Gymnosperms are most abundant in the pollen samples, which can be explained by their distribution mechanisms, which favor exceptionally wide transport (Hopkins, 1950; Traverse and Ginsburg, 1966; Heusser and Balsam, 1977). The position of the drilled core in several kilometer distances to the shore (Harzhauser et al., 2008; Kern et al., 2012a) also plays a role. *Pinus* is excluded here from any environmental reconstruction because it occurs today in very different vegetation zones and altitudes. Other *Pinaceae* such as *Picea* and *Abies* may indicate elevated mountainous regions, such as the close-by Alps (Fauquette et al., 1999; Jiménez-Moreno et al., 2008), which were located less than 100 km from the studied site (Magyar et al., 1999; Harzhauser et al., 2004, 2008). Mid-altitudinal elements are represented by *Tsuga* and *Cathaya* (Jiménez-Moreno et al., 2008; Jiménez-Moreno, 2010), although their recent distribution is not restricted to such environments. This closed vegetation may have been interrupted by more open areas, where *Poaceae* dominated and where rivers flowing into the lake transported numerous riparian elements into the lake (e.g. *Salix*, *Fraxinus*, *Sparganium/Typha*) (Chmura and Liu, 1990; Denk et al., 2001). These vegetation belts correspond fully to the Tortonian vegetation surrounding Lake Pannon as described in several previous studies (e.g. Kovar-Eder et al., 2002, 2006; Harzhauser et al., 2008; Jiménez-Moreno et al., 2008; Kováčová et al., 2011; Kern et al., 2012b).

### 5.3. Pollen zonation

No major turnover of the general vegetation type is indicated in our record (Fig. 3a). This is no surprise with respect to the short time span of only two millennia covered by the core. Nevertheless, the contribution of certain taxa to the spectra changes considerably along the record. A Tiliagraph cluster analysis (Grimm, 2004) revealed significant changes of sample composition resulting in a cluster-based zonation (Fig. 3a). Since the pollen diversity and the pollen/gram sediment counts do not show any parallels (Fig. 3b), shifts within the pollen percentages are presumably not merely an expression of preservation bias (except for subzone IVb, see below).

Zone I (Fig. 3) starts with a high presence of riparian elements (e.g. *Sparganium* in Fig. 3a; Supplementary Table 1), which then strongly decline, reaching levels below 5% after sample 1526. The forested wetland vegetation, however, represented mainly by *Taxodiaceae*, remained intact. This coincidence strongly points to a decrease of fluvial input, either caused by a decreased water supply or a migration of the river mouth. This, in turn, leads to a decrease in pollen diversity because many taxa grow in the hinterland and reach the lake mainly by fluvial transport (Traverse and Ginsburg, 1966; Heusser and Balsam, 1977; Smirnov et al., 1996; Sun et al., 1999).

Zone II (Fig. 3) extends up to sample 1490 and coincides with a continued decline in pollen diversity. The pollen supply from the hinterland forest and from the *Taxodiaceae* wetlands is high, yielding high pollen/gram sediment values. The vegetation composition was rather

uniform, including a huge amount of altitudinal elements such as *Abies*, *Cathaya* and *Tsuga* along with otherwise rare gymnosperms (e.g. *Sciadopitys*, Cupressaceae). Single positive outliers in the pollen/gram ratio may represent events in certain years. Considering the overall rareness of riverine elements and the fact that the most abundant pollen are distributed by wind, these events could be interpreted as several strong wind events rather than as phases of increased runoff. The extreme peaks represent the highest pollen numbers. The average values, however, are higher in pollen zone III.

Within zone III (Fig. 3), the overall plant diversity and the Taxodiaceae vegetation remain rather constant. Although single elements such as *Abies* and *Cathaya* become less abundant, the number of *Picea*, *Tsuga*, hinterland forest vegetation (especially *Carya* and *Fagus*) and the Poaceae increases strongly. This shift in composition could indicate a slight change of the source area, either due to a change in the dominant wind direction or an increase in riverine influx, which fits to several small peaks in the *Sparganium*/*Typha* counts.

Zone IV (Fig. 3) is divided into 2 subzones, ranging from samples 1468–1433 and 1432–1414. Subzone IVa is characterized by high levels of *Picea*, *Cathaya* and Poaceae, while in the pollen/gram counts, the amount of *Pinus* and the contribution by forest elements drop significantly at the base of the upper subzone. Low pollen diversity, pollen/gram values and dinoflagellates/gram values coincide here. Therefore, taphonomic bias might have influenced the record in this case. Especially between samples 1440 and 1430, the lowest pollen/gram sediment values and the lowest diversity values were recorded even robust pollen, such as *Abies* or *Tsuga*, decreases. Nevertheless, the Taxodiaceae, which indicate close-by wetland, remain abundant; this could also point to less wind input during this phase in addition to the taphonomic signal. This is followed by the onset of subzone IVb and an increase in diversity and pollen/gram counts. Hinterland forest elements and all Pinaceae and Poaceae again increase, showing a distinct contribution by far-distance pollen input.

This trend persists into the pollen zone V (Fig. 3; samples 1413–1391). Forest elements, *Picea* and *Abies* and the pollen/gram sediment number continue to increase strongly. Pollen diversity remains stable, but percentages of the hinterland forest reach the highest values; this forest type outcompetes the altitudinal plants.

In conclusion, the pollen record suggests rather unaltered vegetation conditions around the lake during the observed time span. Variations in the pollen spectra are therefore interpreted merely as shifts of the pollen supply into the lake, mainly by changing wind conditions and/or runoff.

#### 5.4. Surface water conditions deduced from dinoflagellate cysts

Dinoflagellate cysts are indicators for the lake surface water conditions (Fig. 4). For Lake Pannon deposits, this group is often difficult to interpret due to the marine origin of Lake Pannon and the subsequent autochthonous evolution of its biota. Many of the genera are today typically found in open marine settings. Nevertheless, some Holocene counterparts are documented from the Black Sea, the Marmara Sea, the Caspian Sea or the Aral Sea, where several species became adapted to brackish water conditions (e.g. Kouli et al., 2001; Mudie et al., 2002, 2004, 2007, 2011; Marret et al., 2004, 2007; Leroy et al., 2007; Londeix et al., 2009; Leroy and Albay, 2010). Especially the dominance of *Spiniferites* in all samples is known from the modern Marmara Sea, where it may account for more than 80% of the dinoflagellate assemblages (Londeix et al., 2009). This high amount of *Spiniferites* was documented by Harzhauser et al. (2008) to have been established in Lake Pannon shortly after a major rise in the lake level. The turning point from coastal to “offshore” conditions, marked by increasing *Impagidinium* and *Spiniferites* values, is recorded at the Hennesdorf section about 40–50 cm below the lowermost part of this core in sample 1540 (Harzhauser et al., 2008). The overall consistently high values of both taxa within our samples therefore indicate a stable lake level without major shifts (Fig. 4) (Dale, 1996; Marret and Zonneveld, 2003).

Another significant element is *Selenopemphix*, which is commonly found in river mouths (e.g. Patterson et al., 2005; Holzwarth et al., 2007). Especially *S. nephroides* has an affinity to eutrophic coastal settings and zones of high productivity (Marret and Zonneveld, 2003; Sorrel et al., 2006). The distinctive drop of *Selenopemphix* up to sample 1500 thus potentially indicates a decrease in freshwater influx (Fig. 4) (Patterson et al., 2005; Holzwarth et al., 2007). This decline is partly compensated by increasing but still low values of the “open-water” taxon *Impagidinium*. In Lake Pannon, a rise of *Impagidinium* was documented to frequently coincide with deepening events (Sluijs et al., 2005; Harzhauser et al., 2008; Kern et al., 2012a). However, the rather moderate increase in the Hennesdorf core might rather point to less river inflow and thus comparatively more oligotrophic conditions, as preferred by *Impagidinium* (Zonneveld, 1995; Dale, 1996). At this level (Fig. 4), the amount of heterotrophic dinoflagellates (Round Brown Cyst (RBC) and Protoperidinioid cyst A) decreases, which points to a decline in surface water nutrients.

This situation quickly changes, as indicated by a strong rise of the absolute dinoflagellates/gram values, which culminates during pollen zone III (Fig. 4). During this phase, brackish but nutrient-rich surface water conditions prevailed. *Pyxidiniopsis*, a taxon well known from the modern brackish Black Sea (Leroy et al., 2007), attains stable high values. This taxon tolerates salinities between 3 and 7 psu in the modern Baltic Sea (Leroy et al., 2007), has its optimum from 7 to 12 psu and becomes rare at salinities exceeding 13 psu (Marret et al., 2007).

From a peak at the border to pollen zone IVa (sample 1471) the values of Protoperidinioid cyst A strongly drop to the benefit of *Impagidinium*. This supports a switch back to more oligotrophic conditions (Zonneveld et al., 2009). Also the RBC drop to their lowest abundance, pointing to a drop in surface water nutrients. Soon after, another turnover occurred in pollen zone IVb, where a rise of Protoperidinioid cysts and a lagged rise of RBC took place. Zone V starts with a second maximum of dinoflagellates abundance, and the high amount of *Selenopemphix* suggests strongly increasing riverine influence towards the top.

#### 5.5. The lake bottom

##### 5.5.1. Ostracods and molluscs

The ostracods of Lake Pannon have been intensively studied in numerous papers (e.g. Gross, 2004; Gross et al., 2008, 2011; Harzhauser et al., 2008; Kern et al., 2012b). A taxonomic analysis of the ostracods from core samples from Hennesdorf (Harzhauser et al., 2008) documented that the species composition remained roughly constant despite strong changes in total abundance. A poor oxygen supply on the lake bottom caused a low-diversity assemblage with only five dominating taxa (*Cyprideis*, *Hemicytheria*, *Lineocypris*/*Caspionella*, *Amplocypris*, *Loxoconcha*). Low bottom water oxygenation and rare nutrient supply strongly constrained growth and success of ostracod populations in Lake Pannon (Harzhauser et al., 2008; Gross et al., 2011; Kern et al., 2012a). The most prolific conditions for ostracod settling were established during deposition of the lower part of the core up to c. sample 1520 (Fig. 5). The conditions were clearly degenerating already in this interval as indicated by the negative trend. This culminates in the very low abundances from sample 1520 onwards, interrupted only by short recovering phases (samples 1510–1500, 1475–1460, 1450–1440). The conditions improved again in the top (above sample 1400), with increasing number of ostracods.

Molluscs occur as isolated shells or as discrete shell-accumulations. These represent autochthonous assemblages of dreissenid bivalves comprising only very few or even single generations, as shown in Harzhauser and Mandic (2004) for the same locality. Generally, molluscs are absent from most samples, indicating hostile conditions for bivalve settlement. Only three phases of more or less continuous settlement are documented (samples 1540–1530, 1474–1461,

1441–1438). They reflect oxygenized bottom water conditions and ample food supply.

### 5.5.2. Geochemistry and geophysics

Geochemical and geophysical measurements do not simply reflect different sediment compositions because the lithology is constant along the studied core.

The natural gamma radiation measurements (GR) detect the presence of radioactive isotopes emitted by potassium-, uranium- and thorium-bearing minerals (Blum et al., 1997). These are transported into the lake mainly by wind or river waters (see Kern et al., 2012a for references). The magnetic susceptibility (MS) is frequently interpreted in an analogous way based on the presence of carrier minerals such as magnetite and pyrrhotite. Nevertheless, the simple interpretation as a function of detrital input has been questioned by the frequent occurrence of greigite in Lake Pannon (Babinszki et al., 2007; Vasiliev et al., 2010). This iron-sulfide is formed under dysoxic conditions in the first centimeters below the lake bottom sediment surface by microbial reactions (Roberts et al., 2011). Thus, the detected MS signal may resemble a combined signal of input, microbial activity and bottom water conditions. Consequently, the original signal may be altered after sedimentation, and the high-frequency signals as revealed by ostracods and GR are lost (Kern et al., 2012a; Fig. 5). A general rise of values occurs between samples 1480 and 1470. As the input-determined GR remains at an overall similar average in that interval, the rise of the MS may possibly be affected by microbial activity within the sediment. This low-oxygen scenario fits also to the very poor ostracod assemblages.

Interpreting the geochemistry of the samples is complex because studies on comparable brackish environments are rare (e.g. Berner, 1984; Sampei et al., 1997; Reischenbacher et al., 2007; Gross et al., 2011). The main source of sulfur in lake deposits is inorganic sulfates and organic sulfur compounds (e.g. Holmer and Storkholm, 2001). These are transferred into organic sulfur mainly by bacterial activity under oxygen-depleted conditions (Goldhaber and Kaplan, 1974; Berner, 1984; Schoonen, 2004). Typically, fine-grained iron-sulfide is formed in the sediment by bacteria (e.g. pyrite and greigite) (Holmer and Storkholm, 2001; Egli, 2004; Pan et al., 2004), which may have been a common process in Lake Pannon (Babinszki et al., 2007; Vasiliev et al., 2010). Compared with organic sulfur, the organic matter content in lakes is higher (Berner, 1984; Holmer and Storkholm, 2001). The organic matter comprises lipids, carbohydrates, proteins and other biological components originated from the lake biota and the surroundings (Meyers, 2003). Total organic carbon (TOC) is the most common proxy to describe the amount of organic matter and as an indicator of productivity (Cohen, 2003; Meyers, 2003). A covariance between TS and TOC was recorded from nearshore deposits of Lake Pannon as result of organic matter input (Gross et al., 2011). Reischenbacher et al. (2007) documented that algal blooms within a Miocene Alpine lake caused similar covariance. This straightforward response is missing in the Hengersdorf core, pointing to a more complex mechanism. Generally elevated sulfur values in the lower half of the core point to high bacterial activity and poor oxygenation at this level. This interpretation is supported by the near absence of benthos. Moreover, the TOC/TS ratio is frequently used as a proxy for freshwater input (Berner, 1984; Sampei et al., 1997; Reischenbacher et al., 2007). This is because the dissolved sulfate supply is strongly limited in freshwater systems compared to brackish/marine ones (Holmer and Storkholm, 2001). The even higher TOC/TS ratio above sample 1430 is also considered to reflect freshwater input.

The calcium carbonate-equivalent (c-equi) is usually interpreted to reflect autochthonous precipitation. Rantisch et al. (2004), however, documented the influence of detrital input from the hinterland on this proxy. Especially along the western shores of Lake Pannon, dolomite and limestone from the Calcareous Alps constitute a major source of

detrital carbonate. A second main factor is the oxygenation of the lake bottom, which influences autochthonous carbonate precipitation.

In the middle part of the section (samples 1490–1465) the c-equi values are high. During this phase, sulfur displays top peaks, magnetic susceptibility increases to a higher level and the natural gamma radiation is strong. In combination with the higher c-equi, all four proxies indicate more intense input of hinterland-derived particles. Another comparable phase of high calcium carbonate-equivalent values occurs between samples 1455 and 1440, again coinciding with high MS values (Fig. 5). A difference is the low TOC and the well-established ostracod populations, suggesting better oxygenation.

### 5.6. General trends

The ecological and environmental data of the various proxies allow a detailed interpretation of the lake record. These are discussed based on the zonation suggested by the pollen data (Fig. 3a); all the information is summarized in Fig. 7.

#### 5.6.1. Zone I (samples 1540–1526)

The high abundance of *Selenophemphix* as well as the peak of TOC/TS ratio suggests strong freshwater inflow into Lake Pannon. This is supported by the presence of river-associated plants (e.g. *Sparganium/Typha*, *Fraxinus*), the high pollen diversity and the high input of organic material as well as a high amount of detrital carbonate. A significant change in the lake level can be excluded because the overall dinoflagellate record is typical for “offshore” settings of Lake Pannon and because the core starts clearly above a major transgressive event described in Harzhauser et al. (2008). The rapid decline of all these proxies within zone I suggests a drop of riverine influx up to sample 1526 (Fig. 7), which defines the boundary between pollen-zones I and II. During the whole ~200-year-long phase, the lake bottom waters were well oxygenated with ample nutrient supply, resulting in the establishment of large ostracod and mollusc populations. This interpretation is in agreement with the pollen data, which clearly document a gradual decrease of riverine elements (see above).

#### 5.6.2. Zone II (samples 1525–1490)

The bottom water oxygenation deteriorated distinctly during the initial 50 years of zone II. Molluscs vanished completely aside from a single layer, and the ostracod populations declined to very low levels and repeatedly collapsed completely. These conditions stimulated the activity of sulfur bacteria, which is expressed in initially increasing MS values and multiple peaks of sulfur. The low TOC/TS ratio also indicates low oxygen conditions and a lack of freshwater inflow into the brackish lake (Fig. 7). Simultaneously, the surface conditions changed. High nutrient levels in the surface waters during the first 200 years of zone II, indicated by an increase of heterotrophic dinoflagellates, are replaced by increasingly oligotrophic conditions in the following 300 years, when *Impagidinium* rose and heterotrophs slightly decreased (Fig. 7). Thus, at that stage, the lake was probably stratified with a poorly oxygenized and hostile hypolimnion (Harzhauser and Mandic, 2004; Reischenbacher et al., 2007; Harzhauser et al., 2008; Roberts et al., 2011).

Although the pollen diversity declined, the number of pollen/gram rose especially due to an increase of the wind-distributed hinterland forest elements and altitudinal trees such as *Abies*, *Cathaya*, *Tsuga* and *Picea*. Thus, transport by wind was probably the major source for pollen, while the riparian elements are nearly missing.

#### 5.6.3. Zone III (samples 1489–1468)

The poorly oxygenized lake bottom conditions of zone II persisted throughout most of zone III. The ostracod record indicated repeated phases of habitable conditions, promoting the development of short-lived populations for several decades. The TOC/TS ratio, however, remained rather low. Phases of high ostracod abundance coincide with

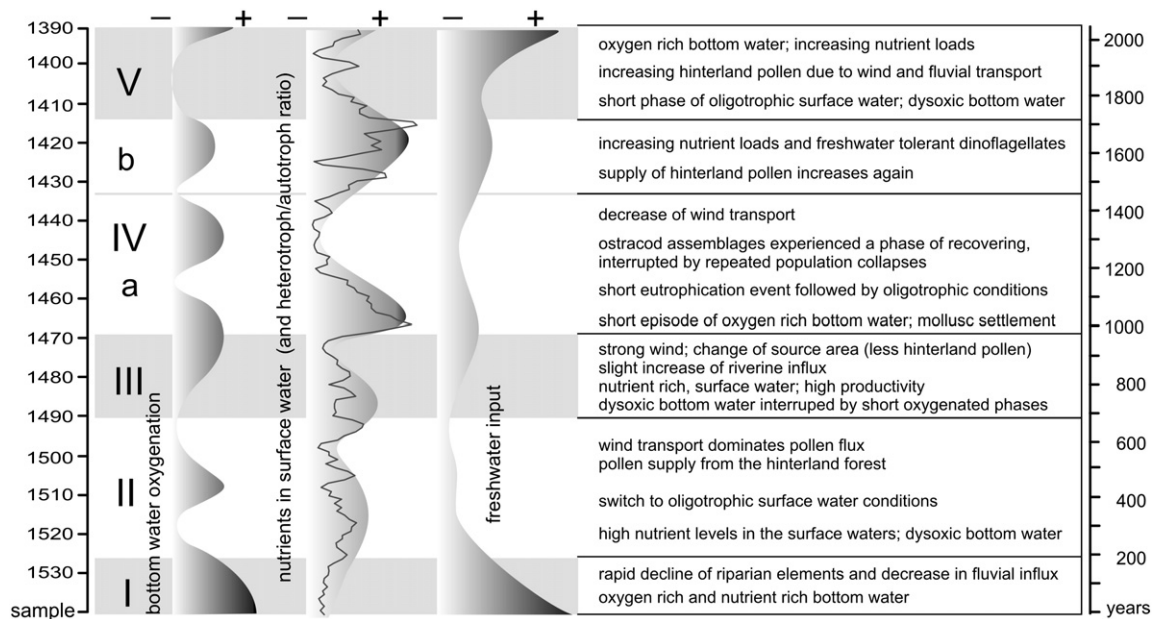


**Fig. 7.** Simplified overview of the major environmental changes as indicated by the various proxies and tentative interpretation of the bottom water oxygenation (ostracods, molluscs, TOC/S, TS), nutrient load (geochemistry, dinoflagellates) and freshwater input (riparian vegetation, freshwater dinoflagellates, sediment input). Changes of environmental parameters occurred on a decadal to centennial scale. Shifts in wind direction and/or intensity seem to have played a major role.

negative peaks in the otherwise high TOC level. The sulfur record also fluctuated; it has several peaks next to steeply rising magnetic susceptibility (Fig. 5). As in zone II, the lake was probably stratified, but episodically epilimnetic conditions became established. This culminated in a short phase around the boundary between zones III and IV in which mollusc coquinas are frequent, suggesting oxygenized lake bottom waters for approximately one century (Fig. 7; Holmer and Storkholm, 2001; Harzhauser and Mandic, 2004; Reischenbacher et al., 2007; Harzhauser et al., 2008; Gross et al., 2011).

The lake surface conditions did not change in the transition from zone II to III. The highest numbers of dinoflagellates/gram document prolific conditions with numerous multi-species blooms. High productivity is reflected by a high percentage of protoperidinioids, which out-compete most other heterotrophs, while the autotrophic *Impagidinium* slightly declines (Fig. 7). Highest numbers of pollen/gram – in combination with a rapidly rising number of forest tree pollen, high amounts of altitudinal elements and *Pinus* – are significant. A rapid succession of peaks in the pollen/gram record suggests repeated wind events, which caused considerable pollen transport. Wind could also stimulate the input of hinterland-derived detritic particles as indicated by the strongly rising carbonate equivalent and rather stable, elevated levels of gamma radiation.

#### 5.6.4. Zone IV (samples 1467–1414)

Based on the pollen record this zone is subdivided into two sub-zones at the boundary of samples 1432/1433. This border coincides with a low in the pollen/gram ratio and is marked by a change from a higher amount of incoming wetland vegetation to hinterland and altitudinal elements. Although all these rise again towards the end of the second subzone, especially *Abies*, *Fagus*, *Pterocarya*, *Celtis* and also *Pinus* have negative peaks around sample 1433. A comparable separation of the zone is indicated by the TOC/TS record, which increases slightly above the subzone-boundary. Moreover, the last phase of mollusc settlement occurs slightly before the boundary (Fig. 7).

Subzone IVa starts with a considerable peak in heterotroph dinoflagellates and low amounts of the autotrophs *Spiniferites* and *Impagidinium* (Fig. 7). This is followed by a strong decline of heterotrophs up the subzone boundary coincides with higher

amounts of autotroph *Pyxidopsis*, indicating lowered salinities and a switch to more oligotrophic conditions. Simultaneously, the ostracod assemblages experienced a recovery phase, interrupted by repeated population collapses of less than 5 decades duration. The longer episodes of bottom water oxygenation (c. samples 1450–1440) might also account for the increasing sulfur recycling and very low TOC values (Fig. 7).

The bottom water oxygenation during subzone IVa might have caused some taphonomic bias within the palynomorphs because the dinoflagellate/gram and the pollen/gram values are both very low. Below the sediment surface, dysoxic conditions prevailed, leading to constant high magnetic susceptibility values. A complete breakdown of the ostracod populations close to this subzone's boundary, due to low oxygen conditions, again correlates with higher values of sulfur.

Within subzone IVb the heterotrophs take over again (Fig. 7) and *Pyxidopsis* declines slightly; ostracods recover on a low level, and TOC and GR increase. The strongest change is indicated by the TOC/TS ratio, which switches to very high values that persist into the subsequent zone V; this suggests a general shift in water chemistry towards less brackish conditions during the last 150 years of zone IV (Leroy et al., 2007; Marret et al., 2007; Reischenbacher et al., 2007).

#### 5.6.5. Zone V (samples 1413–1391)

The uppermost zone is short but appears to consist of two differing parts. The lower part, representing ~100 years, is characterized by a considerable increase in dinoflagellates/gram values but declining number of heterotrophs. Simultaneously, the pollen/gram values slightly decrease. On the lake bottom, conditions deteriorated and ostracods displayed a severe crisis with the lowest abundance of the whole sequence, which coincides with declining MS values in the initial phase of zone V. Molluscs were also unable to settle the lake bottom. Therefore, this interval might correspond to a strongly stratified lake with rather oligotrophic surface water conditions with flourishing autotrophs. The slightly increasing freshwater discharge on the lake surface fostered rising levels of the oligohaline to freshwater-related *Pyxidopsis* (Fig. 7). The absence of noteworthy nutrient input and the lack of benthos caused relatively low amounts of organic sulfur, which is thus missing for bacteria activity (Fig. 7). Within the upper part of zone V the

heterotrophs recovered and *Selenopemphix* increased strongly. On the lake bottom, ostracod populations established again and the total carbon and the carbonate content of the sediment increased. This indicates a considerable higher nutrient level at the same time along with well oxygenized bottom conditions. A high sediment and nutrient input, signalized additionally by higher GR values. These conditions might reflect the re-establishment of riverine influx at some distance away, which also accounts for the possibly delayed strong increase of hinterland forest and higher altitudinal elements along with a rise in the abundance of marsh-associated taxa such as *Nyssa* and *Taxodioideae*. Correspondingly, the high TOC/TS values throughout this zone support this interpretation of decreasing salinity due to increased freshwater supply (Fig. 7).

## 5.7. Influence of solar cycles on the paleoenvironment

### 5.7.1. Filtered records

As the REDFIT spectra detect two dominant frequencies (Fig. 6), the corresponding Gaussian filters were applied to the data (Fig. 8) because the direct impact of these variations is difficult to detect within the raw data. Specifically, the Gaussian bandpass filter integrated to AnalySeries program (Paillard et al., 1996) was used to extract the dominant spectral components. The bandwidth was thereby set to cover the maximum possible area of a peak in the power spectrum. The upper frequency interval (0.12–0.13; 8.3–7.7 cm; 114.2–105.4 years) is represented in *Cathaya*, *Poaceae*, total sulfur and the carbonate content. The two pollen peaks at 0.12 (*Cathaya* and *Poaceae*) result in fully comparable filtered signals with low expressions in the lower half of the core (especially in pollen zone II, Fig. 3a) and an increasingly stable and prominent signal in the upper part. This pattern is also comparable to the filtered carbonate content, which expresses lower intensities at the same levels (Fig. 8). The fourth proxy within this frequency window is total sulfur. The filtered signal is roughly the opposite of the previously discussed pollen curves, with highest amplitudes in the pollen zones I and II. These repetitive changes of *Cathaya*, *Poaceae*, total sulfur and the carbonate content can therefore be linked to the upper Gleissberg cycle.

The lower frequency window with several peaks occurs between 0.16 and 0.267 (6.3–3.8 cm or 85.6–51.3 years). The dinoflagellate taxon *Impagidinium* (0.185 frequency; 5.41 cm; 74.1 years) and RBC (0.186 frequency; 5.37 cm; 73.7 years) show comparable filtered curves, starting with a low intensity in zone I, followed by a strong rise in zone II. Both again display a low amplitude interval in the transition from zone III to IV, which is longer in *Impagidinium*. At the top (mainly pollen zone V), there is another decrease within the *Impagidinium* signal, which is again only weakly reflected in the Round Brown Cysts values. The ostracods (mean value of 0.16 frequency; 6.3 cm; 85.6 years) display only vague parallels with the dinoflagellate signal. Zones I and II are characterized by moderately intense frequencies, and zone III nearly lacks any significant cycles. Above, the signal becomes prominent in zone IV and fades out thereafter.

Some resemblance is also displayed by *Fagus* (0.17 frequency; 5.8 cm; 80.6 years) with a low-amplitude phase at the transition from zone II to III and comparatively stable signals below. No parallels with these signals are expressed in the filtered GR signal (0.167 frequency; 6.0 cm; 82.0 years). It starts with insignificant cycles in zones I and II, rises strongly in zone III when all other proxies have the lowest amplitude signals, and remains prominent thereafter. The highest frequency cycles are detected in the GR record and the Protoperidinioid cysts. The gamma radiation reflects a significant signal filtered at a frequency of 0.21 (4.7 cm; 65.2 years), which remains constant overall with a less intense signal at the transition from zone I to II and in the upper part of subzone IVa. The Protoperidinioid cysts (0.267 frequency; 3.8 cm; 51.3 years), in contrast, start with low values throughout zones I and II, followed by high amplitudes in zone III. Zone IVa is characterized by moderate amplitudes followed by a high phase during zones VIb

and V. Although these filtered records behave individually in most parts, their duration fits the lower Gleissberg cycle.

### 5.7.2. Environmental considerations

The fluctuations in the studied proxies reflect changes of the lake bottom conditions (TS, ostracods), sediment input (GR, carbonate equivalent), surface water conditions (*Impagidinium*, RBC, Protoperidinioid) and terrestrial vegetation (*Cathaya*, *Poaceae*, *Fagus*). Due to the rather short sequence studied, a clear interpretation of the effect of the solar cycles on each environmental aspect is difficult. The dinoflagellates *Spiniferites* and *Impagidinium* display moderate fluctuations with positive and negative peaks within slightly less than one century. These fluctuations might thus be related with the lower Gleissberg cycle. A comparable modulation is observed for the ostracod assemblages and the TS record, although their repetitive signal fits better to the upper Gleissberg cycle as expressed in the filtered records. Despite this suggestion of a possible link, the evidence is not compelling.

Nevertheless, although the data were filtered at slightly shifting frequency centers, the resulting patterns display several similarities with comparable low and high amplitude intervals and equal turning points (Fig. 8). Since all these proxies are independent from each other, representing partly different paleoenvironments, this modulation suggests a common forcing mechanism. The small-scale variations of each signal occur with a rhythm representing either the lower or the upper Gleissberg solar cycle. Therefore, a solar origin appears to be most likely. This implies that the imprint of solar forcing in the records may switch from one dominating solar cycle to another: fluvial transport is an unlikely mechanism to explain most parts of the record (except for the base and the very top; Fig. 7). Therefore, these variations in transport may be best explained by changes in the wind-derived input. Model experiments of Friis-Christensen and Svensmark (1997) have demonstrated the solar radiance most likely controls cloud cover. As a consequence, clouds cause different patterns of rainfall and sunlight reaching the surface, leading to unequal heating and evaporation on land and water. Thus, sun activity and cloud formation determine the wind activity, especially on the continent and in particular at land/water interfaces such as seas or huge lakes like Lake Pannon (Friis-Christensen and Svensmark, 1997).

## 5.8. Modulation of the Gleissberg cycles

Considering the additionally detected longer cyclicities by Kern et al. (2012a) at the same core (Fig. 1), the quasi-periodic 1000-year and 1500-year cycles are the most dominant. Therefore, the filtered 1000-year and 1500-year signals of the ostracod and MS record of Kern et al. (2012a) were used as target curves for the herein-described shorter records. This comparison reveals that the signal modulation of the herein-studied proxies often coincides with one of these longer periodicities (Fig. 8). Especially the *Impagidinium*, Round Brown Cysts and the GR (0.21) signals display a strong 1000-year modulation, which is further visible in the Protoperidinioid signal. Otherwise, the 1500-year periodicity behaves similarly to the *Cathaya*, *Poaceae*, carbonate contents and ostracod records and seems also to be present in the TS signals.

This clustering suggests a strong modulation by the 1000-year solar cycle on lake surface-inhabiting dinoflagellates and might be considered as a “lake cycle”. Shifts between oligotrophic versus eutrophic conditions are the most reliable explanation for this cyclicity. Fluctuating nutrient input would also fit to the strong similarities with the GR record. *Fagus* partly shows an influence of the 1000-year cycle, but this connection is unclear.

The second group, modulated by the 1500-year cycle, suggests a forcing of the transport mechanism from the hinterland as mainly pollen and sediment input proxies are affected. Changing intensity of transport into the lake and/or lake bottom oxygenation also modifies the TS signal and the carbonate content. Both clearly constrain ostracod abundances. The 1500-year cycle might be referred to as a “land cycle”.

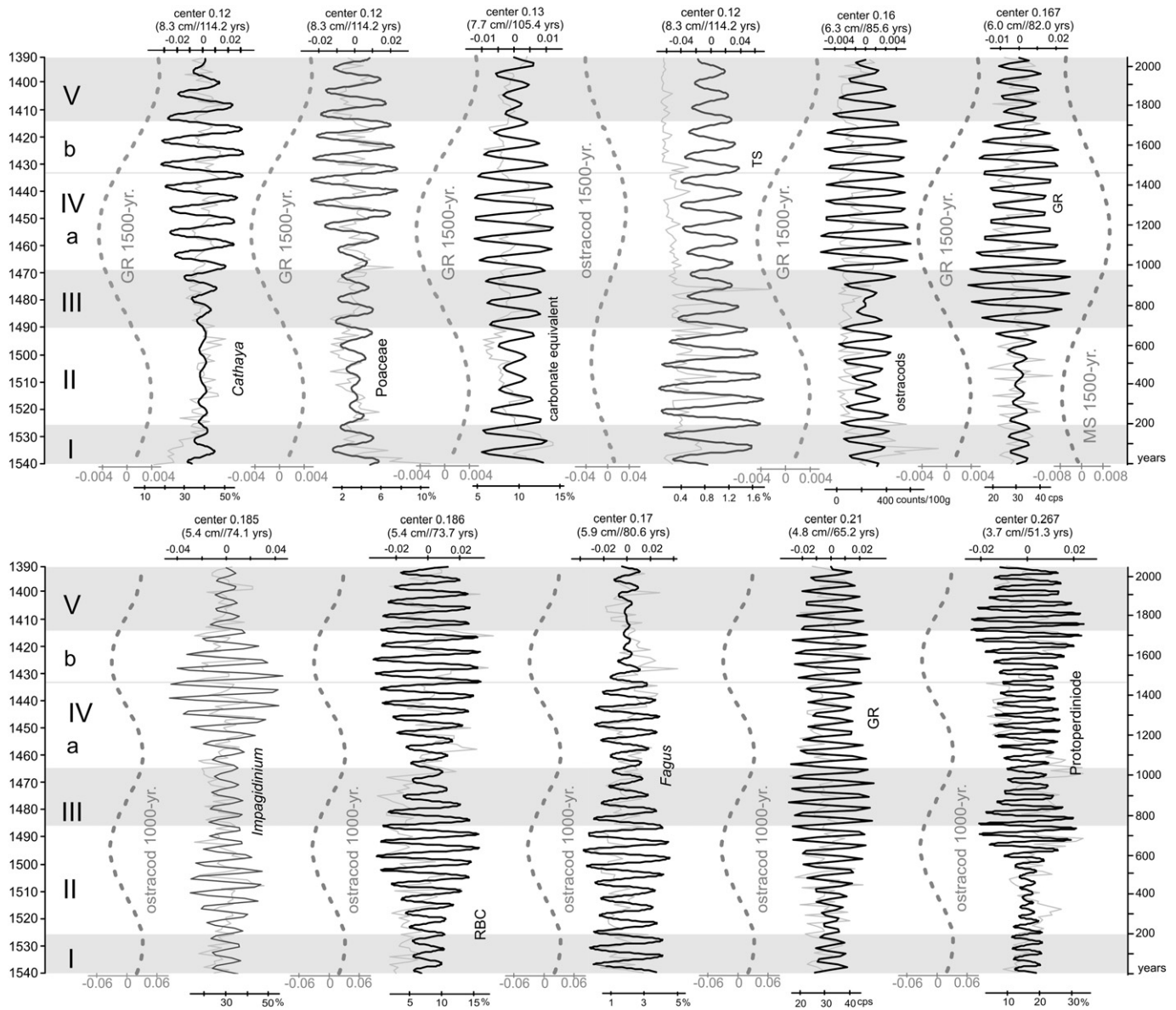


**Fig. 8.** Gaussian filters were applied to selected proxies, which revealed significant peaks in the REDFIT periodograms. The filtered data are superimposed over the raw data of each proxy. The frequency center used for filtering is given on top and transferred to distance and time, showing the signal's repetition frequency. The modulation is compared with 1000-year and 1500-year cycles of the identical core interval detected in the longer ostracod and MS records presented in Kern et al. (2012a) (see Fig. 1); Abbreviations used: GR = natural gamma radiation, TS = total sulfur, MS = magnetic susceptibility, RBC = Round Brown Cysts.

Still, the 1500-year cycle is an “Earth-system-immanent-cycle” and not directly linked to solar forcing (see Bond et al., 2001; Bard and Frank, 2006; Debret et al., 2007 and Kern et al., 2012a for discussion). Therefore, this clear influence on Late Miocene environmental proxies suggests a much more complex interplay between solar forcing and Earth's climate. The changes in wind-triggered input into the lake may result in shifts in dust (detritic carbonate) and pollen transport into the lake. These shifts affect the life in the lake distinctly more than the surrounding vegetation and explain why the overall vegetation did not change significantly. Moreover, the lake surface-dwelling dinoflagellates and the lake bottom-inhabiting ostracods will react more or less in phase with any environmental change, while large parts of the terrestrial vegetation will respond with some delay (e.g. trees and other perennial plants). Despite the minor changes in cloud cover and/or wind intensity, changes of the early Tortonian climate were not intense enough to force changes in the vegetation during this very short period of roughly 2000 years.

## 6. Conclusion

High-frequency environmental changes in and around paleo-Lake Pannon are documented for two millennia of Late Miocene time (Kern et al., 2012a) based on terrestrial and aquatic (planktic) palynomorphs, benthic ostracods and molluscs, and a set of geochemical and geophysical data. These proxies allow a comparison of coeval environmental shifts in the surroundings of the lake, including its forested hinterland, with surface and bottom water conditions (Fig. 7). The overall vegetation did not significantly change during the observed interval. Similarly, the lake level remained rather stable. Nevertheless, several phases can be separated, illustrated by cluster analysis of pollen data, suggesting considerable differences in pollen transport (Fig. 7).

During the first phase (pollen zone I) of slightly more than 200 years, fluvial influx is detected by a higher input of river-associated vegetation and the occurrence of freshwater-tolerant

dinoflagellates. This resulted in a high TOC/TS ratio and in well-oxygenated bottom water conditions as suggested by a large population of ostracods and molluscs. During the following ~500 years (pollen zone II), riverine influx ceased and pollen transport was mainly wind triggered because most of the pollen originate from hinterland forests and even mountainous areas (Fig. 3b). Surface water conditions switched from eutrophic towards more oligotrophic ones and dysoxic bottom waters developed (Fig. 7). These conditions promoted the activity of sulfur bacteria in the lake sediment, as indicated by high sulfur values, a low TOC/S ratio and the increasing magnetic susceptibility. Extraordinarily high pollen/gram sediment counts reflect several wind events which transported wind dispersed pollen into the lake. This trend is further enhanced during the following ~300 years (pollen zone III), but the decline of hinterland elements may indicate a change in the source area. The high input coincides with ample nutrient supply in the surface waters and blooms of heterotrophic dinoflagellates, while bottom waters remained poorly oxygenized. The conditions fluctuated strongly during the subsequent ~700 years (pollen zone IV). A short phase of epilimnic bottom conditions is followed by a succession of dysoxic phases. This situation was interrupted by a 150-year-long phase of well-oxygenated bottom conditions, which caused some taphonomic bias in the palynomorphs. Additionally, low amounts of dinoflagellates coincide distinctly with this oligotrophic phase. Overall, the contribution by wind transport seems to have declined and phases of high hinterland input alternate with intervals of predominant contribution from the close by wetlands. During the last phase (pollen zone V), bottom water conditions improved distinctly after a short dysoxic phase, and moderate fluvial influx was re-established.

Several of these changes occur simultaneously in many proxies and display repetitive patterns when examined with spectral analysis (Fig. 6). These appear in frequencies of 55–82 and 110–123 years, which suggest the influence of lower and upper Gleissberg cycles; this corroborates the results of Kern et al. (2012a), which were based on a much longer core interval of 6 m. Due to the shortness of the core (1.5 m = 150 data points) and the irregular duration of solar cycles, only a selection of proxies indicated solar imprints. Most likely, these observed changes were linked to wind intensity and probably direction. In reference to the pollen spectra, this might document the influence of these solar cycles on prevailing weather conditions, but not climate itself. This could be partly explained by feedback mechanisms between solar energy and cloud formation (Friis-Christensen and Svensmark, 1997). Moreover, both frequency bands of the Gleissberg cycle are modulated by higher-order cycles such as the solar originated 1000-year cycle and the quasi-periodic Earth-system-immanent 1500-year cycle, which is apparently independent of the sun's activity. Especially, the long trend in windiness fits to the 1000-year modulation and might explain its prevalence in hinterland proxies in parts of the studied sequence. Therefore, our data suggest that high-resolution studies of Miocene deposits are powerful tools to detect high-frequency environmental changes in a resolution, which so far has been studied mainly in Holocene records.

Supplementary data to this article can be found online at <http://dx.doi.org/10.1016/j.palaeo.2012.12.005>.

## Acknowledgments

This study was supported by the FWF grant P21414-B16. We thank Dipl.-Ing. Hermann Sammer and the Wienerberger AG for providing access to the clay pit Hennesdorf and for their friendly support during field work. Furthermore, we want to thank Anton Englert, Anton Fürst, Franz Topka, Andy Leggat and Lisa Schmidinger for core preparation, sample processing and counting of the ostracods. We thank Martin Gross for background information concerning geophysics and geochemistry. This paper contributes to the NECLIME network.

## References

- Averyanov, L.V., Phan, E.L., Nguyen, T.H., Nguyen, S.K., Nguyen, T.V., Pham, T.D., 2009. Preliminary observations of native *Glyptostrobus pensilis* (Taxodiaceae) stands in Vietnam. *Taiwania* 54 (3), 191–212.
- Babinszki, E., Márton, E., Kiss, L.F., 2007. Widespread occurrence of greigite in the sediments of Lake Pannon: implications for the environment and magnetostratigraphy. *Palaeogeography, Palaeoclimatology, Palaeoecology* 252, 626–636.
- Bard, E., Frank, M., 2006. Climate change and solar variability: what's new under the sun? *Earth and Planetary Science Letters* 248, 1–14.
- Beer, J., Blinov, A., Bonani, G., Finkel, R.C., Hofmann, H.J., Lehmann, B., Oeschger, H., Sigg, A., Schwander, J., Stauffer, T., Stauffer, Suter, M., Wölfli, W., 1990. Use of  $^{10}\text{Be}$  in polar ice to trace the 11-year cycle of solar activity. *Nature* 347, 164–166.
- Beer, J., Mende, W., Stellmacher, R., 2000. The role of the sun in climate forcing. *Quaternary Science Reviews* 19, 403–415.
- Berner, R.A., 1984. Sedimentary pyrite formation: an update. *Geochimica et Cosmochimica Acta* 48, 605–615.
- Blum, P., Rabaute, A., Gaudon, P., Allan, J.F., 1997. Analysis of natural gamma-ray spectra obtained from sediment cores with the shipboard scintillation detector of the Ocean Drilling Program: example from leg 156. *Proceedings of the Ocean Drilling Program, Scientific Results* 156, 183–195.
- Bond, G., Kormer, B., Beer, J., Muscheler, R., Evans, M.N., Showers, W., Hoffmann, S., Lottiband, R., Hadjas, I., Bonani, G., 2001. Persistent solar influence on North Atlantic Climate during the Holocene. *Science* 294, 2130–2136.
- Britton, R.H., Crivelli, A.J., 1993. Wetlands of southern Europe and North Africa: Mediterranean wetlands. In: Whigham, D.F., Dykijová, D., Hejný, S. (Eds.), *Handbook of Vegetation Science, Wetlands of the World I: Inventory, Ecology and Management*. Kluwer Academic Publishers, Dordrecht, pp. 129–194.
- Bruch, A.A., Utescher, T., Alcalde Olivares, C., Dolakova, N., Ivanov, D., Mosbrugger, V., 2004. Middle and Late Miocene spatial temperature patterns and gradients in Europe – preliminary results based on palaeobotanical climate reconstructions. *Courier Forschungsinstitut Senckenberg* 249, 15–27.
- Bruch, A.A., Utescher, T., Mosbrugger, V., Gabrielyan, I., Ivanov, D.A., 2006. Late Miocene climate in the circum-Alpine realm – a quantitative analysis of terrestrial palaeofloras. *Palaeogeography, Palaeoclimatology, Palaeoecology* 238, 270–280.
- Charvátová, I., 2000. Can origin of the 2400-year cycle of solar activity be caused by solar inertial motion? *Annales Geophysicae* 18, 399–405.
- Chmura, G.L., Liu, K.-B., 1990. Pollen in the lower Mississippi River. *Review of Palaeobotany and Palynology* 64, 253–261.
- Cini Castagnoli, G., Taricco, C., Alessio, S., 2005. Isotopic record in a marine shallow-water core: imprint of solar centennial cycles in the past 2 millennia. *Advances in Space Research* 35, 504–508.
- Claud, C., Cagnazzo, C., Keckhut, P., 2008. The effect of the 11-year solar cycle on the temperature in the lower stratosphere. *Journal of Atmospheric and Solar-Terrestrial Physics* 70, 2031–2040.
- Cohen, A.S., 2003. *Paleolimnology – The History and Evolution of Lake Systems*. Oxford University Press, New York.
- Dale, B., 1996. Dinoflagellate cysts ecology: modelling and geological applications. In: Jansonius, J., McGregor, D.C. (Eds.), *Palynology: Principles and Applications*. American Association of Stratigraphic Palynologists Foundation, Dallas, pp. 1249–1276.
- Damon, P.E., Sonett, C.P., 1991. Solar and terrestrial components of the atmospheric c-14 variation spectrum. In: Sonett, C.P., Giampapa, M.S., Methews, M.S. (Eds.), *The Sun in Time*. The University of Arizona, Tucson, pp. 360–388.
- de Jager, C., Duhau, S., van Geel, B., 2010. Quantifying and specifying the solar influence on terrestrial surface temperature. *Journal of Astronomical and Solar-terrestrial Physics* 72, 926–937.
- Debret, M., Bout-Roumazeilles, V., Grousset, F., Desmet, M., McManus, J.F., Massei, N., Sebag, D., Petit, J.-R., Copard, Y., Trentesaux, A., 2007. The origin of the 1500-year climate cycles in Holocene North-Atlantic records. *Climate of the Past* 3, 569–575.
- Debret, M., Sebag, D., Crosta, X., Massei, N., Petit, J.-R., Chapron, E., Bout-Roumazeilles, V., 2009. Evidence from wavelet analysis for a mid-Holocene transition in global climate forcing. *Quaternary Science Reviews* 28, 2675–2688.
- Denk, T., Frotzler, N., Davitashvili, N., 2001. Vegetational patterns and distribution of relict taxa in humid temperate forests and wetlands of Georgia (Transcaucasia). *Biological Journal of the Linnean Society* 72, 287–332.
- Di Rita, F., 2011. A possible solar pacemaker for Holocene fluctuations of salt-marsh in southern Italy. *Quaternary International*. <http://dx.doi.org/10.1016/j.quaint.2011.11.030>.
- Egli, R., 2004. Characterization of individual rock magnetic components by analysis of remanence curves. 3. Bacterial magnetite and natural processes in lakes. *Physics and Chemistry of the Earth* 29, 869–884.
- Fauquette, S., Clauzon, G., Suc, J.-P., Zheng, Z., 1999. A new approach for paleoaltitude estimates based on pollen records: example of the Mercantour Massif (southeastern France) at the earliest Pliocene. *Earth and Planetary Science Letters* 170, 35–47.
- Friis-Christensen, E., Svensmark, H., 1997. What do we really know about the sun-climate connection? *Advances in Space Research* 20, 913–921.
- Garcin, Y., Williamson, D., Taieb, M., Vincens, A., Mathé, P.-E., Majule, A., 2006. Centennial to millennial changes in maar-lake deposits during the last 45,000 years in tropical Southern Africa (Lake Masoko, Tanzania). *Palaeogeography, Palaeoclimatology, Palaeoecology* 329, 334–354.
- Gleissberg, 1939. *Observatory* 62, 158.
- Goldhaber, M.B., Kaplan, I.R., 1974. The sulfur cycle. In: Goldberg, E.D. (Ed.), *The Sea*, vol. 5. John Wiley & Sons, London, pp. 569–655.

- Gray, L.J., Beer, J., Gellar, M., Haigh, J.D., Lockwood, M., Matthes, K., Cubasch, U., Fleitmann, D., Harrison, G., Hood, L., Lutenbacher, J., Meehl, G.A., Shindell, D., van Geel, B., White, W., 2010. Solar influence on climate. *Review of Geophysics* 48, RG4001.
- Green, O.R., 2001. *A Manual of Practical Laboratory and Field Techniques in Palaeobiology*. Kluwer Academic Publishers, Dordrecht.
- Grimm, E.C., 2004. Tilia and TG View Version 2.0.2. Illinois State Museum, Research and Collector Center.
- Gross, M., 2004. Zur Ostracodenfauna (Crustacea), Paläoökologie und Stratigraphie der Tongrube Mataschen (Unter-Pannonium, Steirisches Becken, Österreich). *Joannea Geologie und Paläontologie* 5, 49–129.
- Gross, M., Minati, K., Danielopol, D.L., Piller, W.E., 2008. Environmental changes and diversification of *Cyprideis* in the Late Miocene of the Styrian Basin (Lake Pannon, Austria). *Senckenbergiana lethaea* 88, 161–181.
- Gross, M., Piller, W.E., Scholger, R., Gitter, F., 2011. Biotic and abiotic response to palaeoenvironmental changes at Lake Pannon's western margin (Central Europe, Lake Miocene). *Palaeogeography, Palaeoclimatology, Palaeoecology* 312, 181–193.
- Hammer, Ø., Harper, D.A.T., Ryan, P.D., 2001. PAST: Palaeontological Statistics Software package for education and data analysis. *Palaeontologia Electronica* 4 (1) (9 pp.).
- Harzhauser, M., Mandic, O., 2004. The muddy bottom of Lake Pannon. *Palaeogeography, Palaeoclimatology, Palaeoecology* 204, 331–352.
- Harzhauser, M., Mandic, O., 2008. Neogene lake systems of Central and South-Eastern Europe: faunal diversity, gradients and interrelations. *Palaeogeography, Palaeoclimatology, Palaeoecology* 260, 417–434.
- Harzhauser, M., Daxner-Höck, G., Piller, W.E., 2004. An integrated stratigraphy of the Pannonian (Late Miocene) in the Vienna Basin. *Austrian Journal of Earth Sciences* 95 (96), 6–19.
- Harzhauser, M., Kern, A., Soliman, A., Minati, K., Piller, W.E., Danielopol, D.L., Zuschin, M., 2008. Centennial- to decadal scale environmental shifts in and around Lake Pannon (Vienna Basin) related to a major Lake Miocene lake level rise. *Palaeogeography, Palaeoclimatology, Palaeoecology* 270, 102–115.
- Heusser, L., Balsam, W.L., 1977. Pollen distribution in the Northeast Pacific Ocean. *Quaternary Research* 7, 45–62.
- Holmer, M., Storkholm, P., 2001. Sulphate reduction and sulphur cycling in lake sediments: a review. *Freshwater Biology* 46, 431–451.
- Holzwarth, U., Esper, O., Zonneveld, K., 2007. Distribution of organic-walled dinoflagellate cysts in shelf surface sediments of the Benguela upwelling system in relationship to environmental conditions. *Marine Micropaleontology* 64, 91–119.
- Hopkins, J.S., 1950. Differential flotation and deposition of coniferous and deciduous tree pollen. *Ecology* 31, 633–641.
- Hoyt, D.V., Schatten, K.H., 1997. The Role of the Sun in Climate Change. Oxford University Press, Oxford, U.K. (279 pp.).
- Hoyt, D.V., Schatten, K.H., 1998. Group sunspot numbers: a new solar activity reconstruction. *Solar Physics* 179, 189–219.
- Incarbona, A., Ziveri, P., Di Stefano, E., Lirer, F., Mortyn, G., Patti, B., Pelosi, N., Sprovieri, M., Tranchida, G., Vallefucio, M., Albertazzi, S., Bellucci, L.G., Bonanno, A., Bonomo, S., Censi, P., Ferraro, L., Giuliani, S., Mazzola, S., Sprovieri, R., 2010. The impact of the Little Ice Age on Cocolithopores in the Central Mediterranean Sea. *Climate of the Past* 6, 795–805.
- Jarvis, D.I., Clay-Poole, S.T., 1992. A comparison of modern pollen rain and vegetation in southwestern Sichuan Province, China. *Review of Palaeobotany and Palynology* 75, 239–258.
- Jiménez-Moreno, G., 2006. Progressive substitution of a subtropical forest for a temperate one during the middle Miocene climate cooling in Central Europe according to palynological data from cores Tengeic-2 and Hidas-53 (Pannonian Basin, Hungary). *Review of Palaeobotany and Palynology* 142, 1–14.
- Jiménez-Moreno, G., 2010. Cathaya: a gymnosperm most likely indicating a mid-altitude coniferous forest during the Neogene in the European area. 8th European Palaeobotany–Palynology Conference, Budapest, Hungary, 126.
- Jiménez-Moreno, G., Suc, J.-P., 2007. Middle Miocene latitudinal climate gradient in Western Europe: evidence from pollen records. *Palaeogeography, Palaeoclimatology, Palaeoecology* 253, 208–225.
- Jiménez-Moreno, G., Fauquette, S., Suc, J.-P., 2008. Vegetation, climate and paleoaltitude reconstructions of eastern alpine mountain ranges during the Miocene based on pollen records from Austria, Central Europe. *Journal of Biogeography* 35, 1638–1649.
- Kern, A.K., Harzhauser, M., Piller, W.E., Mandic, O., Soliman, A., 2012a. Strong evidence for the influence of solar cycles on a Late Miocene Lake system revealed by biotic and abiotic proxies. *Palaeogeography, Palaeoclimatology, Palaeoecology* 329–330, 124–136.
- Kern, A.K., Harzhauser, M., Soliman, A., Piller, W.E., Gross, M., 2012b. Precipitation driven decadal scale decline and recovery of wetlands of Lake Pannon during the Tortonian. *Palaeogeography, Palaeoclimatology, Palaeoecology* 317–318, 1–12.
- Kouli, K., Brinkhuis, H., Dale, B., 2001. *Spiniferites cruciformis*. A fresh water dinoflagellate cyst? *Review of Palaeobotany and Palynology* 113, 273–286.
- Kováčová, M., Deláková, N., Kováč, M., 2011. Miocene vegetation pattern and climate change in the northwestern Central Paratethys domain (Czech and Slovak Republic). *Geologica Carpathica* 62, 251–266.
- Kovar-Eder, J., Schwarz, J., Wójcicki, J.J., 2002. The predominantly aquatic flora from Pellendorf, Lower Austria, late Miocene, Pannonian — a systematic study. *Acta Palaeobotanica* 42, 125–151.
- Kovar-Eder, J., Kvaček, Z., Martinetto, E., Roiron, P., 2006. Late Miocene to Early Pliocene vegetation of southern Europe (7–4 Ma) as reflected in the megafossil plant record. *Palaeogeography, Palaeoclimatology, Palaeoecology* 238, 321–339.
- Kovar-Eder, J., Jechorek, H., Kvaček, Z., Parashiv, V., 2008. The integrated plant record: an essential tool for reconstructing Neogene zonal vegetation in Europe. *Palaia* 23, 97–111.
- Kunzmann, L., Kvaček, Z., Mai, D.H., Walther, H., 2009. The genus *Taxodium* (Cupressaceae) in Palaeogene and Neogene of Central Europe. *Review of Palaeobotany and Palynology* 153, 153–183.
- Kvaček, Z., 2007. Do extant nearest relatives of thermophile European Cenozoic plant elements reliably reflect climatic signal? *Palaeogeography, Palaeoclimatology, Palaeoecology* 253, 32–40.
- Leroy, S.A.G., Albay, M., 2010. Palynomorphs of brackish and marine species in cores from the freshwater Lake Sapanca, NW Turkey. *Review of Palaeobotany and Palynology* 160, 181–188.
- Leroy, S.A.G., Marret, F., Gibert, E., Chalié, F., Reyss, J.-L., Arpe, K., 2007. River inflow and salinity changes in the Caspian Sea during the last 5500 years. *Quaternary Science Reviews* 26, 3359–3383.
- Li, K.J., Yun, H.S., Gu, X.G., 2001. Hemispheric variation in solar activity. *The Astrophysical Journal* 554, L115–L117.
- Linder, A., Berchtold, W., 1976. *Statistische Auswertung von Prozentzahlen*. Birkhäuser, Basel, pp. 1–230.
- Lirer, F., Harzhauser, M., Pelosi, N., Piller, W.E., Schmid, H.P., Sprovieri, M., 2009. Astronomically forced teleconnection between Paratethyan and Mediterranean sediments during the Middle and Late Miocene. *Palaeogeography, Palaeoclimatology, Palaeoecology* 275, 1–13.
- Lodge, T.E., 2010. *The Everglades Handbook — Understanding the Ecosystem*. Taylor and Francis Group, Boca Raton. (392 pp.).
- Londeix, L., Herreyre, Y., Turon, J.-L., Fletcher, W., 2009. Last Glacial to Holocene hydrology of the Marmara Sea inferred from a dinoflagellate cyst record. *Review of Palaeobotany and Palynology* 158, 52–71.
- Magyar, I., Geary, D.H., Müller, P., 1999. Paleogeographic evolution of the Late Miocene Lake Pannon in Central Europe. *Palaeogeography, Palaeoclimatology, Palaeoecology* 147, 151–167.
- Marret, F., Zonneveld, K.A.F., 2003. Atlas of modern organic-walled dinoflagellate cyst distributions. *Review of Palaeobotany and Palynology* 125, 1–200.
- Marret, F., Leroy, S., Chalié, F., Gasse, F., 2004. New organic-walled dinoflagellate cysts from recent sediments of Central Asian seas. *Review of Palaeobotany and Palynology* 129, 1–20.
- Marret, F., Mudie, P.J., Aksu, A., Hiscott, R.N., 2007. Holocene dinocyst record of a two-step transformation of the Neoeuxinian brackish water lake into the Black Sea. *Quaternary International* 197, 72–86.
- Meyers, P.A., 2003. Applications of organic geochemistry to paleolimnological reconstructions: a summary of examples from the Laurentian Great Lakes. *Organic Geochemistry* 34, 261–289.
- Mosbrugger, V., Utescher, T., 1997. The coexistence approach — a method for quantitative reconstructions of Tertiary terrestrial palaeoclimate data using plant fossils. *Palaeogeography, Palaeoclimatology, Palaeoecology* 134, 61–86.
- Mudie, P.J., Rochon, A., Aksu, A.E., Gillespie, H., 2002. Dinoflagellate cysts, freshwater algae and fungal spores as salinity indicators in Late Quaternary cores from Marmara and Black seas. *Marine Geology* 190, 203–231.
- Mudie, P.J., Rochon, A., Aksu, A.E., Gillespie, H., 2004. Late glacial, Holocene and modern dinoflagellate cyst assemblages in the Aegean–Marmara–Black Sea corridor: statistical analysis and re-interpretation of the early Holocene Noah's Flood hypothesis. *Review of Palaeobotany and Palynology* 128, 143–167.
- Mudie, P.J., Marret, F., Aksu, A.E., Hiscott, R.N., Gillespie, H., 2007. Palynological evidence for climatic change, anthropogenic activity and outflow of Black Sea water during the late Pleistocene and Holocene: centennial- to decadal-scale records from the Black and Marmara Seas. *Quaternary International* 167–168, 73–90.
- Mudie, P.J., Leroy, S.A.G., Marret, F., Gerasimenko, N., Kholeif, S.E.A., Sapelko, T., Filipova-Marinova, M., 2011. Nonpollen palynomorphs: indicators of salinity and environmental change in the Caspian–Black Sea–Mediterranean corridor. In: Buynevich, I., Yanko-Hombach, V., Gilbert, A.S., Martin, R.E. (Eds.), *Geology and Geoarchaeology of the Black Sea Region: Beyond the Flood Hypothesis*. Geological Society of America Special Paper 473 (pp.).
- Müller, M.J., 1996. *Handbuch ausgewählter Klimastationen der Erde*. Forschungsstelle Bodenerosion Universität Trier, Mertesdorf (Ruwertal).
- Muscheler, R., Beer, J., Vonmoos, M., 2004. Causes and timing of the 8200 yr BP event inferred from the comparison of the GRIP  $^{10}\text{Be}$  and the tree ring  $\Delta^{14}\text{C}$  record. *Quaternary Science Reviews* 23, 2101–2111.
- Ogurtsov, M.G., Nagovitsyn, Y.A., Kocharov, G.E., Jungner, H., 2002. Long-period cycles of the sun's activity recorded in direct solar data and proxies. *Solar Physics* 211, 371–394.
- Paillard, D., Labeyrie, L., Yiou, P., 1996. Macintosh program performs time-series analysis. *Eos, Transaction American Geophysical Union* 77, 379.
- Pan, Y., Deng, C., Liu, Q., Petersen, N., Zhu, R., 2004. Biomineralization and magnetism of bacterial magnetosomes. *Chinese Science Bulletin* 49, 2563–2568.
- Patterson, R.T., Prokoph, A., Chang, A., 2004. Late Holocene sedimentary response to solar and cosmic ray activity influenced climate variability in the NE Pacific. *Sedimentary Geology* 172, 67–84.
- Patterson, R.T., Prokoph, A., Kumar, A., Chang, A.S., Roe, H.M., 2005. Late Holocene variability in pelagic fish scales and dinoflagellate cysts along the west coast of Vancouver Island, NE Pacific Ocean. *Marine Micropaleontology* 55, 183–204.
- Paulissen, W.E., Luthi, S.M., 2011. High-frequency cyclicity in a Miocene sequence of the Vienna Basin established from high-resolution logs and robust chronostratigraphic tuning. *Palaeogeography, Palaeoclimatology, Palaeoecology* 307, 313–323.
- Piller, W.E., Harzhauser, M., Mandic, O., 2007. Miocene Central Paratethys stratigraphy — current status and future directions. *Stratigraphy* 4 (2/3), 71–88.
- Rantisch, G., Müller, N., Ebner, F., 2004. Geochemical and mineralogical investigations of Pannonian Sediments on the clay put Mataschen (Styrian Basin, Austria). *Joannea Geologie und Paläontologie* 5, 219–230.

- Raspov, O., Dergachev, V.A., Kolström, T., 2004. Periodicity of climate conditions and solar variability derived from dendrochronological and other palaeoclimatic data in high latitudes. *Palaeogeography, Palaeoclimatology, Palaeoecology* 209, 127–139.
- Raspov, O.M., Dergachev, V.A., Esper, J., Kozyreva, O.V., Frank, D., Ogursov, M., Kolström, T., Shao, X., 2008. The influence of the de Vries (200-year) solar cycle on climate variations: results from the Central Asian Mountains and their global link. *Palaeogeography, Palaeoclimatology, Palaeoecology* 259, 6–16.
- Reischenbacher, D., Rifelj, H., Sachsenhofer, R.F., Jelen, B., Čorić, S., Gross, M., Reichenbacher, B., 2007. Early Badenian paleoenvironment in the Lavanttal Basin (Mühldorf Formation, Austria): evidence from geochemistry and paleontology. *Austrian Journal of Earth Sciences* 100, 202–229.
- Rigozo, N.R., Nordemann, D.J.R., Ether, E., Zanandrea, A., Gonzalez, W.D., 2002. Solar variability effects studied by tree-ring data wavelet analysis. *Advances in Space Research* 29, 1985–1988.
- Rigozo, N.R., da Silva, H.E., Nordemann, D.J.R., Echer, E., de Souza, Pereira, Echer, M., Prestes, A., 2008. The Medieval and Modern Maximum solar activity imprints in tree ring data from Chile and stable isotope records from Antarctica and Peru. *Journal of Atmospheric and Solar–Terrestrial Physics* 70, 1012–1024.
- Roberts, A.P., Chang, L., Rowan, C.J., Horng, C.-S., Florindo, F., 2011. Magnetic properties of sedimentary greigite ( $\text{Fe}_3\text{S}_4$ ): an update. *Review of Geophysics* 49, RG1002.
- Sampei, Y., Matsumoto, E., Kamei, T., Tokioka, T., 1997. Sulfur and organic carbon relationship in sediments from coastal brackish lakes in the Shimane peninsula district, southwest Japan. *Geochemical Journal* 31, 245–262.
- Schoonen, M.A.A., 2004. Mechanisms of sedimentary pyrite formation. In: Amend, J.P., Edwards, K.J., Lyons, T. (Eds.), *Sulfur biogeochemistry: past and present: The Geological Society of America Special Papers* 379, pp. 117–134 (Boulder, CO.).
- Schulz, M., Mudelsee, M., 2002. REDFIT: estimating red-noise spectra directly from unevenly spaced paleoclimatic time series. *Computers & Geosciences* 28, 421–426.
- Sluijs, A., Pross, J., Brinkhuis, H., 2005. From greenhouse to icehouse; organic-walled dinoflagellate cysts as paleoenvironmental indicators in the Paleogene. *Earth-Science Reviews* 68, 281–315.
- Smirnov, A., Chmura, G.L., Lapointe, M.F., 1996. Spatial distribution of suspended pollen in the Mississippi River as an example of pollen transport in alluvial channels. *Review of Palaeobotany and Palynology* 92, 69–81.
- Solanki, S.K., Usoskin, I.G., Kromber, B., Schüssler, M., Beer, J., 2004. Unusual activity of the Sun during recent decades compared to the previous 11,000 years. *Nature* 431, 1084–1087.
- Sonett, C.P., Suess, H.E., 1984. Correlation of bristlecone pine ring widths and atmospheric  $^{14}\text{C}$  variations: a climate–sun relation. *Nature* 307, 141–143.
- Sorrel, P., Popescu, S.-M., Head, M.J., Suc, J.P., Klotz, S., Oberhänsli, H., 2006. Hydrographic development of the Aral Sea during the last 2000 years based on a quantitative analysis of dinoflagellate cysts. *Palaeogeography, Palaeoclimatology, Palaeoecology* 234, 304–327.
- Stuiver, M., Braziunas, T.F., 1989. Atmospheric  $^{14}\text{C}$  and century-scale solar oscillations. *Nature* 338, 405–408.
- Stuiver, M., Braziunas, T.F., 1993. Sun, ocean, climate and atmospheric  $^{14}\text{CO}_2$ , an evaluation of causal and spectral relationships. *The Holocene* 3, 289–305.
- Sun, X., Li, X., Beug, H.-J., 1999. Pollen distribution in hemipelagic surface sediments of the South China Sea and its relation to modern vegetation distribution. *Marine Geology* 156, 211–226.
- Taricco, C., Ghil, M., Alessio, S., Vivaldo, G., 2009. Two millennia of climate variability in the Central Mediterranean. *Climate of the Past* 5, 171–181.
- Thompson, R.S., Anderson, K.H., Bartlein, P.J., 1999. Atlas of relations between climatic parameters and distributions of important trees and shrubs in North America. US Geological Survey Professional Paper 1650-A.
- Traverse, A., Ginsburg, R.N., 1966. Palynology of the surface sediments of Great Bahamas Bank, as related to water movement and sedimentation. *Marine Geology* 4, 417–459.
- Tsiropoulou, G., 2003. Signatures of solar activity variability in meteorological parameters. *Journal of Atmospheric and Solar–Terrestrial Physics* 65, 469–482.
- Utescher, T., Mosbrugger, V., Ashraf, A.R., 2000. Terrestrial climate evolution in Northwest Germany over the last 25 million years. *Palaios* 15, 430–449.
- Utescher, T., Ivanov, D., Harzhauser, M., Bozukov, V., Ashraf, A.R., Rolf, C., Ubrat, M., Mosbrugger, V., 2009. Cyclic climate and vegetation change in the late Miocene of Western Bulgaria. *Palaeogeography, Palaeoclimatology, Palaeoecology* 272, 99–114.
- Vasiliev, I., de Leeuw, A., Filipescu, S., Krijgsman, W., Kuiper, K., Stoica, M., Briceag, A., 2010. The age of the Sarmatian–Pannonian transition in the Transylvanian Basin (Central Paratethys). *Palaeogeography, Palaeoclimatology, Palaeoecology* 297, 54–69.
- Versteegh, G.J.M., 2005. Solar forcing of climate. 2: Evidence from the past. *Space Science Reviews* 120, 243–286.
- Wilen, B.O., Tiner, R.W., 1993. Wetlands of the United States. In: Whigham, D.F., Dykijová, D., Hejný, S. (Eds.), *Handbook of Vegetation Science, Wetlands of the World I: Inventory, Ecology and Management*. Kluwer Academic Publishers, Dordrecht, pp. 129–194.
- Willard, D.A., Weimer, L.M., Riegel, W.L., 2001. Pollen assemblages as paleoenvironmental proxies in the Florida Everglades. *Review of Palaeobotany and Palynology* 113, 213–235.
- Wolf, R., 1862. *Astronomische Mitteilungen Zürich*, 14.
- Wood, G.D., Gabriel, A.M., Lawson, J.C., 1996. Palynological techniques – processing and microscopy. In: Jansonius, J., McGregor, D.C. (Eds.), *Palynology: Principles and Applications*, vol. 1. American Association of Stratigraphic Palynologists Foundation, Dallas, pp. 29–50.
- Zachos, J., Pagani, M., Sloan, L., Thomas, E., Billups, K., 2001. Trends, rhythms, and aberrations in global climate 65 Ma to present. *Science* 292, 686–693.
- Zonneveld, K.A.F., 1995. Palaeoclimatic and palaeo-ecological changes during the last deglaciation in the Eastern Mediterranean – implications for dinoflagellate ecology. *Review of Palaeobotany and Palynology* 84, 221–253.
- Zonneveld, K.A.F., Chen, L., Möbius, J., Mahmoud, M.S., 2009. Environmental significance of dinoflagellate cysts from the proximal part of the Po-river discharge plume (off southern Italy, Eastern Mediterranean). *Journal of Sea Research* 62, 189–213.
- Zuschin, M., Hohenegger, J., 1998. Subtropical coral-reef associated sedimentary facies characterized by mollusks (Northern Bay of Safage, Red Sea, Egypt). *Facies* 38, 229–254.